TECHNICAL CONTRIBUTIONS

THE MEMORY EFFECT OF THE ISOPHOT-C100 DETECTOR

Ronny Blomme and Mark C. Runacres

Royal Observatory of Belgium, Ringlaan 3, B-1180 Brussel, Belgium

ABSTRACT

The large number of scientific observations in the ISO archive reveals considerable systematics in the detector behaviour, which can be used to improve the data reduction process.

Key words: ISO – C100 – detector model

1. INTRODUCTION

The pixels of the C100 detector show transient behaviour: after a change in flux, the measured signal follows a complicated function of time that only asymptotically goes to the appropriate value (Laureijs et al. 2001, Sect. 4.2.2). In the OLP (Off-Line Processing, version 10.0) the transient part of the signal is simply discarded. Recent versions of PIA (PHOT Interactive Analysis) allow the fitting of transient functions (e.g. offset exponentials) to the data. Such functions have a number of unknown parameters, reflecting our lack of knowledge of the detector.

It is well known however that the values of these fit parameters depend on the flux that was previously measured. This knowledge is included in P32Tools (Tuffs et al. 2002). In a previous paper we showed how one of the fitting parameters of the offset exponential is related to the previous flux (Blomme & Runacres 2002). Other studies that consider this memory effect are given in Acosta-Pulido et al. 2000, del Burgo et al. 2002 and Lari et al. 2002.

2. LONG-TERM BEHAVIOUR

In this section and the next one, we present the results of our study of staring observations (P22, P37, P39), where we look at the first position on the sky after an FCS measurement, or at the FCS measurement that follows a sky observation. Data reduction was done in PIA[1] 9.0.1, supplemented by own routines. We only show results for the central pixel; other pixels show a behaviour that is qualitatively similar.

When there is a change in the flux that falls on the instrument (i.e. a flux step), the detector does not react immediately.

[1] The ISOPHOT data presented in this paper were reduced using PIA, which is a joint development by the ESA Astrophysics Division and the ISOPHOT consortium, with the collaboration of the Infrared Analysis and Processing Center (IPAC) and the Instituto de Astrofísica de Canarias (IAC)

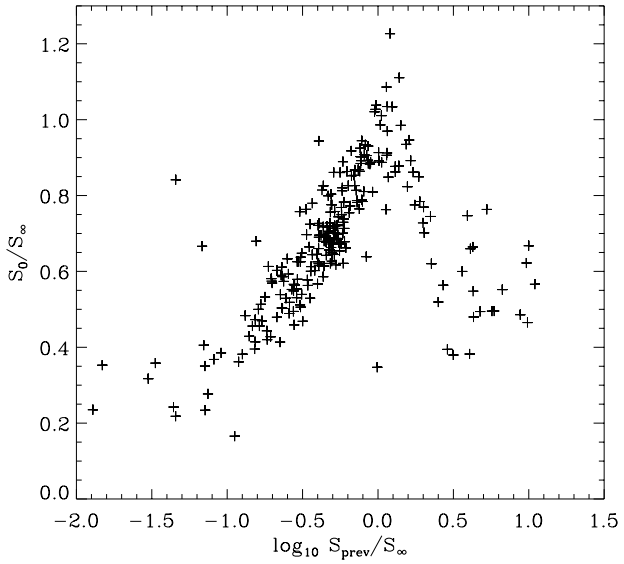

Figure 1. S_0/S_∞ as a function of $\log(S_{\rm prev}/S_\infty)$ for a large number of staring observations from the ISO archive (100 μm filter only).

Instead, the measured signal can be approximated by an offset exponential as a function of time:

$$S(t) = S_\infty + (S_0 - S_\infty) \exp\left(-\frac{t}{\tau_0}\right) \quad (1)$$

The parameters of the offset exponential are highly correlated with the value of the previous flux, as a systematic study of the archive data shows. Fig. 1 shows S_0 as a function of $S_{\rm prev}$, which is the signal corresponding to the previous flux (both normalised to S_∞). This highly systematic effect allows us to reduce the number of parameters in the fitting procedure. We checked that using such "reduced" offset exponential also results in good-quality fits.

3. SHORT-TERM BEHAVIOUR

While an offset exponential fits the data quite well, there are still discrepancies at the start of some observations.

3.1. UPWARD FLUX STEP

Fig. 2 shows that in the case of a large upward flux step, the signal at $t \approx 0$ is less than the offset exponential predicts. These

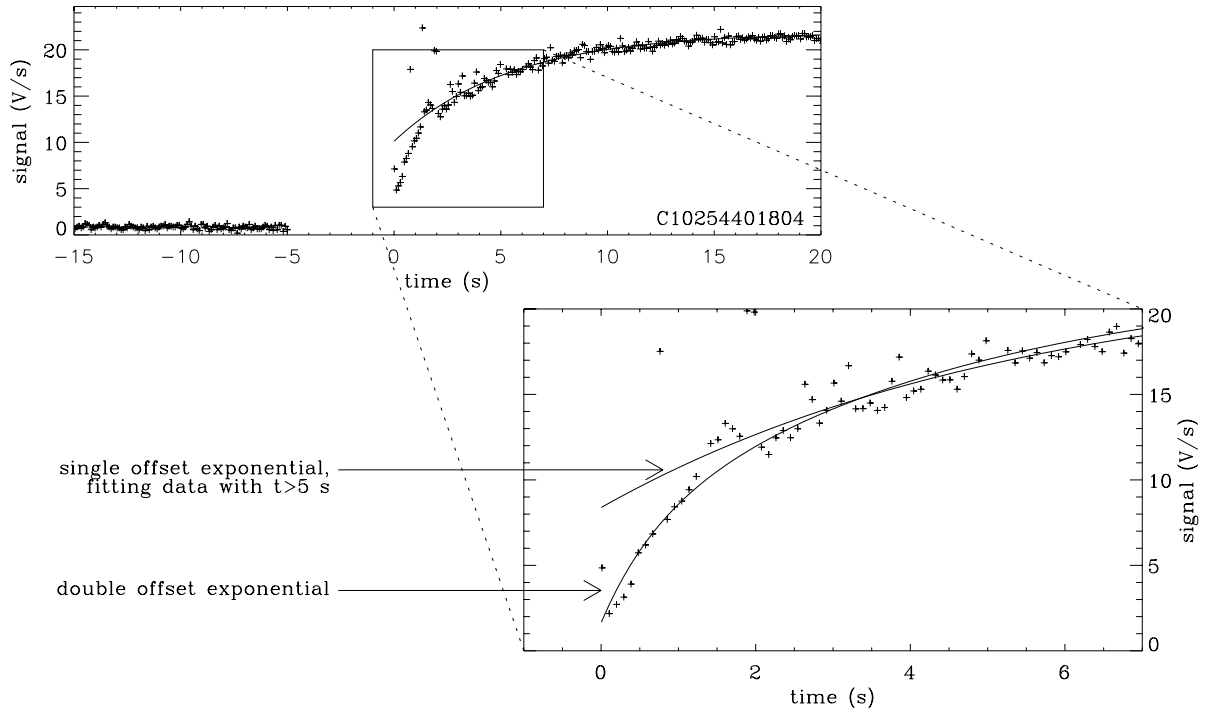

Figure 2. A double offset exponential fits the signals better at $t \approx 0$ than a single offset exponential does.

discrepancies can be considerably reduced by fitting a double offset exponential to the data:

$$S(t) = S_\infty + (S_0 - S_\infty) \exp\left(-\frac{t}{\tau_0}\right) + S_2 \exp\left(-\frac{t}{\tau_2}\right) \quad (2)$$

In this expression, the first exponential describes the long-term behaviour, the second exponential the short-term behaviour.

Again, going through the archive and fitting the observations with this double offset exponential shows a highly systematic trend in the fit parameters (see Fig. 3). Because of systematics such as this, it should be possible to fit a more sophisticated function (double offset exponential) to the observations, without introducing additional parameters.

3.2. Downward flux step

When there is a downward flux step, the behaviour of the signal also deviates from an offset exponential at $t \approx 0$. Again, a double exponential is used to better fit the signal, and a highly systematic trend in the fit parameters is found (see Fig. 4).

4. CONCLUSIONS

The detailed study of the ISOPHOT-C100 scientific data in the archive has already shown considerable systematics in the behaviour of the detector. Further work will certainly reveal more of the systematics. Ideally, this should result in a sophisticated fitting function for the transient behaviour, with only a single unknown parameter: S_∞.

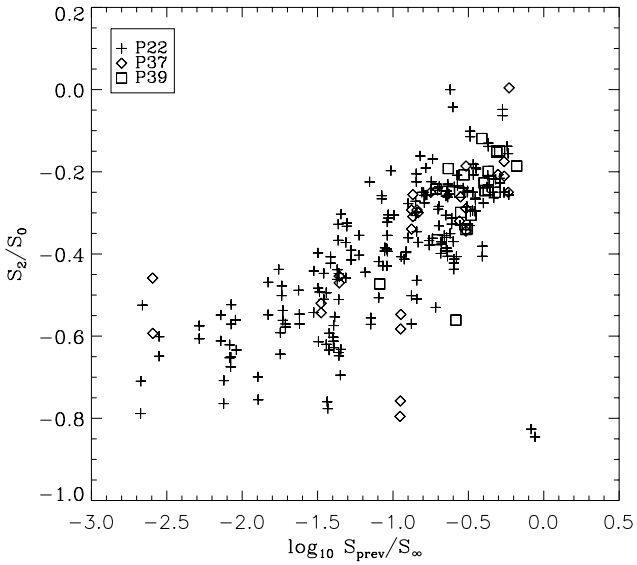

Figure 3. S_2/S_0 as a function of $\log(S_{\rm prev}/S_\infty)$.

While the results presented here concern only staring observations (P22, P37, P39), the short time scale behaviour is also relevant for chopping (e.g. P32) observations.

ACKNOWLEDGEMENTS

This work was funded by ESA-Prodex project no. 13346/98/NL/VJ(ic).

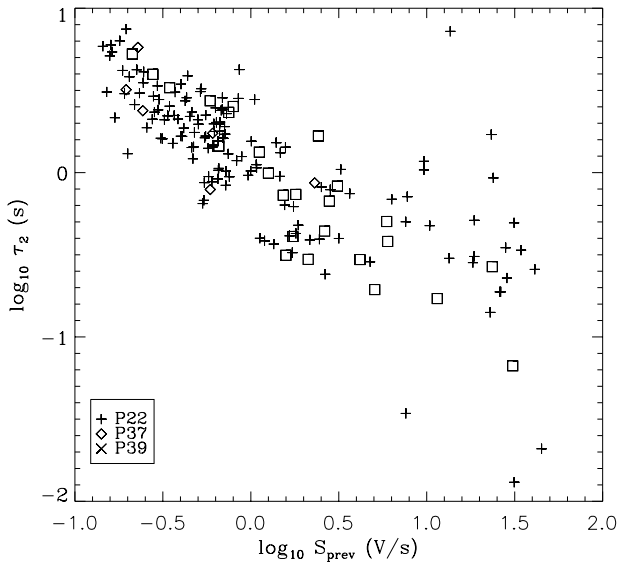

Figure 4. τ_2 *as a function of* S_{prev} *in a log-log plot.*

REFERENCES

Acosta-Pulido J.A., Gabriel C., Castañeda H.O., 2000, Experimental Astronomy 10, 333

Blomme R., Runacres M.C., 2002, in: Proceedings of the *ISOPHOT Workshop on P32 Oversampled Mapping*, ESA SP-482, in press

del Burgo, C., et al., 2002, this volume

Laureijs R.J., Klaas U., Richards P.J., Schulz B., Ábrahám P., 2001, The ISO Handbook. Volume V. PHT, Version 1.2

Lari, C., et al., 2002, this volume

Tuffs R., et al., 2002, in: Proceedings of the *ISOPHOT Workshop on P32 Oversampled Mapping*, ESA SP-482, in press

FREQUENTLY–ASKED QUESTIONS ABOUT FOUKS MODELS AND TRANSIENT CORRECTION METHODS FOR THE ISOCAM LW DETECTOR

Alain Coulais[1,2] **and Alain Abergel**[1]

[1] Institut d'Astrophysique Spatiale, Batiment 121, Université Paris XI, 91405 Orsay cedex, France
[2] LERMA, Observatoire de Paris, 61, Av. de l'Observatoire, 75 014 Paris - France

ABSTRACT

At low temperature and for very low (astrophysical) incoming flux, most of the IR detectors are affected by transient response, which delays the response and can strongly bias the estimated flux. The LW detector of ISOCAM is also affected by such behaviour. It has been shown that an important component of the transient effects of this detector can be described with high accuracy using a non-linear and non-symmetrical model based on pure physics. An inversion method is also available. In this paper, we review the limitations of this model and the known problems occurring with the correction method, and we give advice on how to process the data.

Key words: ISO – CAM, CVF, Fouks model, Si:Ga, transient, memory effect

1. INTRODUCTION

It has been shown (Coulais & Abergel 2000) that, if the gradient between adjacent pixels is small, one model[1] based on the Fouks theory can describe the transients for the LW matrix detector of ISOCAM (Cesarsky et al. 1996) on-board ISO (Kessler et al. 1996) with a very high accuracy. However, several hypotheses and problems are hidden. The goal of this paper is to describe the limitations of both the transient model and the transient correction method.

Section 2 presents the differences between the direct model and the transient correction method. Section 3 details the limits in the direct model, and Sect. 4 the technical difficulties encountered during data processing. The whole section 5 is devoted to the processing of CVF data, which can be difficult for a lot of observations. Finally Sect. 6 outlines briefly the new 3D model which describes the transients for point sources (Fouks et al. 2002).

2. A DIRECT MODEL AND AN INVERSION METHOD

Two main software packages have been developed (Coulais & Abergel 2000) and are actually included in CIA (Gastaud et al. 2002) :

- the *direct* Fouks *model*, which describes the transient of the ISOCAM LW detector for low-contrast illumination (low gradient between adjacent pixels);
- the specific *inversion method* based on the direct model (correction method).

The direct model is able to reproduce the transient response of individual pixels under uniform illumination. The inversion method has been developed to recover the corrected value for each readout. This method works on a readout-by-readout basis, using the pre-history. No parameter is fitted. Up to now, it is considered that the two parameters β, λ of the direct model are constant for each pixel (32×32 maps of β and λ have been provided). This method is sufficiently reliable for most good quality CAM data so it is not necessary to use other information, such as block-by-block constraints or redundancy checking (between adjacent pixels or on the sky).

3. LIMITS IN THE DIRECT MODEL

First we recall[2] several facts about the direct model :

- The direct model describes the transient response of the detector (*short term transient*) well for upward and downward flux steps between a large range of initial and final illumination levels, subject to a quasi-uniform illumination of the matrix array (small gradient between adjacent pixels).
- The direct model does not describe point source transients correctly. The higher the peak flux and the narrower the source profile, the worse the result (Coulais & Abergel 2000; Coulais et al. 2000). A new 3D model for transients of point sources is now available (Fouks et al. 2002, see also Sect. 6).
- The direct model does not at all describe the long term drift (LTD, e.g. TDT 12900101, cf Fig. 1 in Coulais & Abergel 2000) which may occur after the *fast* transient. Following Fouks' theory, the lower the initial level, the longer the long term drift and the higher the actual flux variation (Vinokurov & Fouks 1991). As a matter of fact, it is not possible to model the LTD (see explanations in Coulais & Abergel 2002). A correction method based on the spatial redundancy in raster maps was successfully developed (Miville-Deschênes et al. 2000) to reduce the effects of

[1] The so-called Fouks-Schubert model since it was successfully used for Si:Ga PHOT S and P on ground-based data (Fouks 1995; Fouks & Schubert 1995; Schubert 1995).

[2] It is mentioned in several papers that this model fails in various cases. These cases precisely correspond to conditions where the model is not applicable.

Proceedings of the Symposium *"Exploiting the ISO Data Archive - Infrared Astronomy in the Internet Age"*, 24–27 June 2002, Sigüenza, Spain (C. Gry, S. B. Peschke, J. Matagne et al. eds., ESA SP-511)

LTD and to extract low-contrast structures –like faint interstellar clouds– in raster observations with at least two legs.
- The direct model always gives a monotonous transient response for a block of readouts observing a constant input flux. Moreover, the output of the direct model is always strictly positive (see Coulais & Abergel 2000 for details).
- The direct model does not at all describe the small amplitude oscillations. This effect was clearly exhibited during ground based tests for upward steps at high amplitude (Coulais et al. 2000). A model for in-flight data was studied by Aussel (Priv. Com.) using Fouks' equations (Fouks 1996).
- Up to now, an explanation can always be found when the model and the data disagree. Classical problems are :
  - bad initialization or flagged data used as initialization,
  - missing readouts or time discontinuities,
  - negative mean values and inaccurate dark correction.
- The direct model cannot reproduce glitches, which result from the impact of high energy particles. Glitches are usually classified in three categories (see in Coulais & Abergel 2002 and references therein):
  - instantaneous glitches,
  - faders and
  - dippers.

4. PROBLEMS WITH THE TRANSIENT CORRECTION METHOD

Since the inversion method is based on the direct model, it is obvious that this method cannot correct transients that are not fit by the direct model. Moreover, this method does not test the possible divergences or the consistency of the estimated values of the incoming flux.

4.1. DARK CORRECTION

A dark current correction must be applied to the data (Biviano et al. 1998). It has been observed that the dark current is changing with time over the course of an orbit, but also over the lifetime of ISO (Biviano et al. 1998; Gallais 2001). The accuracy of the dark correction is limited, which can be a problem when using the direct model and the correction method. The closer to zero, the more sensitive to the dark errors. Especially CVF observations close to zero are very sensitive to inaccurate dark subtraction, as detailed in Sect. 5.

If data are very close to zero flux level, or contain negative values after dark correction, the application of the transient correction method may lead to lots of problems. It is difficult to add an arbitrary offset level. This offset must take into account the pixel to pixel variations, one of the biggest effects arises from the fact that the odd/even lines have different dark levels due to the electronics (Vigroux et al. 1993). Sometimes the odd/even effect is clearly visible in the data signal after dark correction. For the CVF with direct and reverse scans, the criterion for the determination of the offset is that it improves the superposition of the two scans. For raster maps, flux steps are mandatory to check the possible range of offset. For a two-step-configuration with the initial level J_0 close to zero and final level $J_1 \gg 0$, it is possible to estimate J_0 with very high accuracy with the help of the direct model, which is strongly non-linear close to zero (see Fig. 4 in Coulais & Abergel 2000).

4.2. NEGATIVE VALUES

Even if the dark level is perfectly estimated, we may have negative values in the data due to noise. The transient correction method can also diverge due to negative values. Since this divergence is not systematic, some simulations have been performed. In simulations, the occurrence of this divergence is very limited and is still unpredictable in positive data where only Gaussian noise is added (mean value in a moving window is positive). The divergence always occurs when the offset level of the dataset is underestimated with negative data (due to the added noise). As a consequence, the lower the flux level in the data, the higher the required accuracy of the dark level to avoid divergence of the transient correction method.

It is clear that one large part of the noise is sampling noise, which is smoothable. Temporal filtering before applying the transient correction can reduce such problems. This modification is not included in the official transient correction in the latest versions of CIA.

4.3. DEGLITCHING

It is better to deglitch the data before applying the transient correction method. Nevertheless the correction method is robust to instantaneous glitches. Any deglitching method is OK (3σ clipping, wavelets (Starck et al. 1999)), except the methods which remove the first readout after a flux step (first readout of an upward step). Two methods can be used to substitute the de-glichted readouts : replace them with the temporal median value (or temporal and spatial median value) or flag them with the undefinded value. The transient correction is able to take into account changing delay between two successive readouts.

We have problems for the glitches with positive (*fader*) and negative tails (*dipper*). With 3σ clipping they remain in the time series and are corrected as transients but they are not. It has been reported (Lari 1997; Rodighiero & Lari 2002; Lari et al. 2002) that such *faders* and *deepers* can be corrected. Such a correction is not available in CIA.

4.4. INITIAL CONDITIONS AND MEMORY EFFECT

One very interesting property of the direct model is that, for each pixel, the whole flux pre-history can be summarized with only one number, corresponding to the output flux before the first readout (details in Coulais & Abergel 2000). For the whole detector, a map "J_{-1}" has to be estimated. Several methods can be used.

When the data are clearly stabilized during the first N readouts, we can use the median value for the J_{-1} map, for each

pixel, for these N readouts. But at low flux level the correction method will create big artifacts for an error in J_{-1}. This is especially true for a CVF measurement, starting at low flux levels.

When the data are not stabilized during the first readouts, the pre-history can be estimated using the direct model. Nevertheless since all the data are now public, a very good solution is to look at the dataset just before the observation in question. If the configuration is the same (i.e. ISOCAM observation using the LW detector) and the time discontinuity is small (to be checked carefully to avoid indeterminate states or saturation), data concatenation is a very efficient way to find J_{-1}.

It should be noticed that, if the J_{-1} map contains negative values for several pixels, the transient correction method diverges systematically for these pixels after a long time ($\sim 10 - 10^3$ readouts). This behavior can be predicted from the analytical equations of the model, and can be easily reproduced with the direct model. Therefore, before applying the transient correction method, it must be checked that J_{-1} does not contain any negative values or zero values.

4.5. Point Sources

Transients for uniform illumination and point sources are indeed processed in the same way. As a result, transient corrections fail for point sources. On raster maps, we frequently see the bright "ghosts" due to inaccurately corrected transients after point sources (e.g. TDT 11301003). A direct model for transients of point sources can now be used (see Sect 6 and Fouks et al. 2002).

4.6. Downward steps

The transient correction method can diverge when going from very high flux levels to very low ones, due to inaccuracy of the β parameter[3] (the instantaneous jump) for some pixels, and also due to the inaccuracy of the dark correction. This effect is linked to the creation of negative values resulting from over-correction of the downward steps, which can create artificially strong memory effects (It is simple to simulate this kind of problem).

5. THE SPECIFIC CASE OF CVF CORRECTION

The transient correction of CVF observations can be more difficult than the one for rasters because the flux levels are frequently very low. The closer to zero, the longer the memory effect. CVF observations are also affected by the limited accuracy of the dark current level : a small error in the faint absolute level can strongly magnify or reduce the transient effects. Furthermore these effects do not linearly depend on the initial level (see Fig. 4 in Coulais & Abergel 2000).

[3] Limitations in the estimation of the fixed parameters (β, λ) were detailed in Coulais & Abergel 2000.

5.1. One-direction CVF scan

A lot of CVF observations consist of only upward or downward scans (in wavelength). When the flux levels of these CVF scans are close to zero (let's say less than a few ADU), one has to be very cautious when processing them because the possible problems with the transient correction method cannot be checked. These problems, like divergence or magnification of the memory effect, are due to an incorrect dark current level. These problems are more critical when starting from a flux level close to zero (generally at the shortest wavelengths).

Simulations help a lot to understand the complex non-linear effects. The problems do not come from the limitations in the model. In any case it is necessary to work on a pixel-by-pixel basis, because of odd/even effects in the dark correction.

5.2. Two-direction CVF scans

For CVFs with bidirectional scans and flux levels close to zero, a much better job can be done than for CVF measurements with only one scan direction (e.g. the CVF on Fig. 10 in Coulais & Abergel 2000). In case of poor transient correction (i.e. the two scans do not overlap after the transient correction), one method to improve the correction is to carefully re-estimate the dark level for each pixel. The idea is to estimate the best offset to be added to the dark level in order to have positive values and to have a perfect overlap of the two scans after transient correction. To fix the best dark level, a dichotomic approach is certainly the best one. In the CIA software are provided not only the correction method but also the direct model. So simulations and corrections can be done.

6. POINT SOURCE TRANSIENT

A direct model was developed (Fouks et al. 2002 and refs. therein) to reproduce the transients of point sources. The accuracy is good enough to describe the transients for each pixel for all forty configurations of ISOCAM (four pixel-fields-of-view(PFOV) and ten filters) except for the four configurations giving the widest PSF : PFOV=1.5 arcsec and filters LW 3, 8, 9 and 10. But for these four cases a second order term improves the agreement between data and model. A first correction method based on this model has been developed for isolated sources (Normand 2002). Examples, problems and limitations are detailed in Fouks et al. 2002.

7. CONCLUSION

The direct model describes the transient response with a high accuracy, for quasi-uniform illumination. Memory effects due to pre-history of the illumination are also accurately described, even at the lowest flux levels (e.g. CVFs). Depending on the integration time, the filter wheel, the lens(PFOV) and the accuracy of the dark model, an accuracy of the transient description of better than 1–2 % can generally be achieved for each readout of most pixels (direct simulation). Unfortunately, the pixels

along the sides (and especially at the edges) cannot be adjusted with a similar accuracy due to boundery effects.

Some difficulties can appear when applying the transient correction method without caution, especially because the model is sensitive to the initial conditions (critical for low flux levels), divergence can occur for negative values, and the errors can propagate. Nevertheless, when the transient correction method is applied to a well prepared dataset (good dark correction, deglitching, correct initialization, ...), the correction accuracy remains at the 3 % error level per readout.

Since the direct model and the correction method are both provided in CIA, it is possible to gain some experience with simulations. One very good final check is to apply the direct model to the artificial dataset to check for some significant difference between the observed and the simulated data.

The CVF observations can be more difficult to correct than the raster observations due to : (1) inaccurate correction for the dark level (2) low flux levels and (3) no flux step is available to constrain properly the initial conditions. The transient model and the transient correction method must not be used to derive the flux of points sources. But a new model and corrections are now available (Fouks et al. 2002).

Finally the correction method developed for the LW detector of ISOCAM can be used for other Si:Ga detectors (e.g. SWS b2 and PHOT, see explanations in Sect. 4 of Coulais & Abergel 2000), and *a priori* should be adaptable to other direct models without difficulties (e.g. the current study for the FTS mode for ASTRO-F).

ACKNOWLEDGEMENTS

AC would like to thank all the people who gave feedback about this work, especially S. Ott, D. Cesarsky, K. Okumura, J. Blommaert, B. Ali, F. Boulanger, M.-A. Miville-Deschêne, P. Chanial, Y. Fuchs, H. Aussel R. Gastaud and C. Joblain. This work was done during a long stay at IAS with financial support from the French CNES.

REFERENCES

Biviano, A. et al.: 1998, *The ISOCAM Dark Current Calibration Report*, Technical report, ISOCAM

Cesarsky, C. J. et al.: 1996, *Astron. Astrophys.* **315**, L32

Coulais, A. and Abergel, A.: 2000, *Astron. Astrophys. Suppl. Ser.* **141**, 533

Coulais, A. and Abergel, A.: 2002, ESA SP-481, in press

Coulais, A., Fouks, B. I., Giovannelli, J.-F., Abergel, A., and Sée, J.: 2000, in M. Strojnik and B. Andresen (eds.), *Infrared Spaceborne Remote Sensing VIII*, Vol. 4131, pp 205–217, SPIE, San Diego, USA

Fouks, B., Coulais, A., and Normand, J.: 2002, this volume

Fouks, B. I.: 1995, *Proceedings of SPIE* **2553**, 489

Fouks, B. I.: 1996, *Proceedings of SPIE* **2817**, 160

Fouks, B. I. and Schubert, J.: 1995, *Proceedings of SPIE* **2475**, 487

Gallais, P.: 2001, in: Proceedings for *The calibration legacy of the ISO Mission'*, Eds.: L. Melcalfe et al. 2003, ESA SP-481

Gastaud, R., Ott, S., Guest, S., Delaney, M., Sam-Lone, J., Starck, J.-L., Ali, B., Landriu, D., Miville-Deschênes, M.-A., Sauvage, M., and Vivares, F.: 2002, ESA SP-481, in press

Kessler, M. F. et al.: 1996, *Astron. Astrophys.* **315**, L27

Lari, C.: 1997, *IRA model for ISOCAM LW transient correction*, Technical report, IRA

Lari, C., Vaccari, M., Fadda, D., and Rodighiero, G.: 2002, this volume

Miville-Deschênes, M.-A., Boulanger, F., Abergel, A., and Bernard, J.-P.: 2000, *Astron. Astrophys. Suppl. Ser.* **146**, 519

Normand, J.: 2002, *Etude et correction des transitoires des sources ponctuelles d'ISOCAM*, Stage de 2ième année Ingénieur, IAS, France

Rodighiero, G. and Lari, C.: 2002, ESA SP-481, in press

Schubert, J.: 1995, *Ph.D. thesis*, Max Planck-Institut für Astronomie, Heidelberg

Starck, J.-L., Abergel, A., et al.: 1999, *Astron. Astrophys. Suppl. Ser.* **134**, 135

Vigroux, L. G., Cesarsky, C. J., Boulade, O., Rio, Y., Perault, M., Abergel, A., Désert, F.-X., Rouan, D., and Lacombe, F.: 1993, *Proceedings of SPIE* **1946**, 281

Vinokurov, L. A. and Fouks, B. I.: 1991, *Sov. Phys. Semicond.* **25(11)**, 1207

RE-ANALYSED STEPS OF THE ISOPHOT CALIBRATION SCHEME: RESET INTERVAL CORRECTION, TRANSIENT CORRECTION, AND BY-PASSING SKY LIGHT SUBTRACTION

Carlos del Burgo[1], **Philippe Héraudeau**[1], **and Péter Ábrahám**[1,2]

[1]Max-Planck Institut für Astronomie, Königstuhl 17, D-69117 Heidelberg, Germany
[2]Konkoly Observatory of the Hungarian Academy of Sciences, P.O. Box 67, H-1525 Budapest, Hungary

ABSTRACT

From all suitable ISOPHOT archive data we have reviewed different instrumental effects for P- and C-detectors and derived new calibration files. We present a re-analysis of the reset interval correction, a new method for the transient correction, and the first correction algorithm for by-passing sky light in FCS measurements performed with the ISOPHOT C-detectors.

Key words: ISO

1. INTRODUCTION

The ISO Legacy Archive (Kessler et al. 2000) has been filled up with data automatically reduced by the On-Line Processing Software (OLP) V.10, and it represents the status of calibration achieved by the end of 2000. Follow-up tests and systematic validation work, however, identified observing modes where the photometric consistency is reduced pointing to possible open issues in the calibration.

One of these modes is the absolute surface brightness photometry with ISOPHOT where a correlation analysis of the surface brightness values measured by ISOPHOT (Lemke et al. 1996) and by COBE/DIRBE (Silverberg et al. 1993) revealed systematic differences between the zero points of the two instruments (Héraudeau et al. 2002). With the aim of clarifying the origin of the zero point differences and improving ISOPHOT's capabilities for sky background studies (like the determination of the Extragalactic Background Light) we launched a large scale calibration project in early 2001. Our strategy was to re-investigate several steps of the ISOPHOT calibration scheme, especially those related to the zero point determination and surface brightness photometry. The first result, a re-analysis of the dark signal, was published by del Burgo et al. (2001).

In the present contribution we present an analysis of three more issues of the ISOPHOT data processing using all suitable archive data. Sect. 2.1 presents a re-analysis of the correction required to harmonize signals taken with different reset interval settings. In Section 2.2 a new signal transient correction method is described. Finally, in Section 2.3 a quantitative analysis of the by-passing sky light is reported for the first time. A full description of all the calibration steps investigated and tests of the final absolute surface brightness accuracies will be presented elsewhere (del Burgo et al. 2002, in preparation).

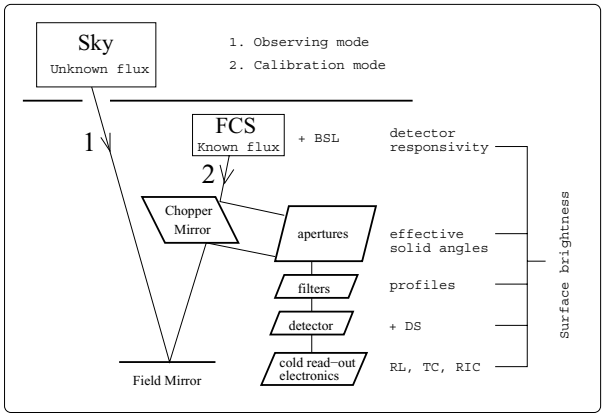

Figure 1. Schematic overview of ISOPHOT observing (1) and calibration (2) modes. Essential elements for the surface brightness reconstruction are shown. Note that the chopper mirror is not used here for beam modulation, but only to feed in the internal reference source beam in a separate measurement. Abbreviations are for by-passing sky light (BSL), dark signal (DS), ramp linearization (RL), transient correction (TC), and reset interval correction (RIC).

2. ISOPHOT DATA PROCESSING

In general each ISOPHOT observation comprises a sky and a heated Fine Calibration Source (FCS) measurement, obtained in observing (staring or raster) and calibration mode, respectively (see Fig. 1). The individual processing steps and the necessary corrections are described in the ISOPHOT Handbook (Laureijs et al. 2002) and marked in Fig. 1. In the following we give a description of the three calibration issues of interest and present our results.

2.1. RE-ANALYSIS OF THE RESET INTERVAL 2.2. CORRECTION

In order to match a large flux range (several decades) to the dynamic range of the AD converters, the reset interval (RI), time between two destructive read-outs, of the integration process had to be adjusted to the expected total incident flux. Measurements of the same source with the same detector, filter and aperture combination but with distinct reset interval setting (RI= 2^n s, where n=-6, -5, ..., 6) yield different signals (see Fig. 2). The reset interval correction converts the signals

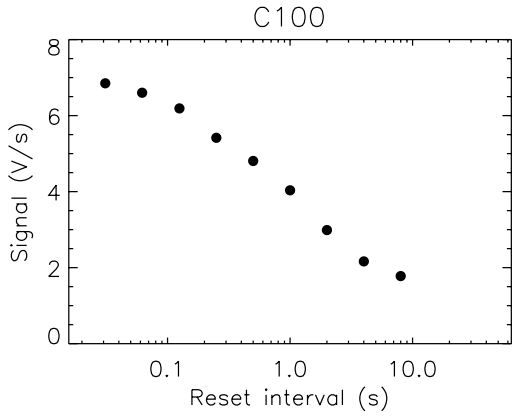

Figure 2. Signal versus reset interval for a constant illumination corresponding to detector C100 (pixel 1).

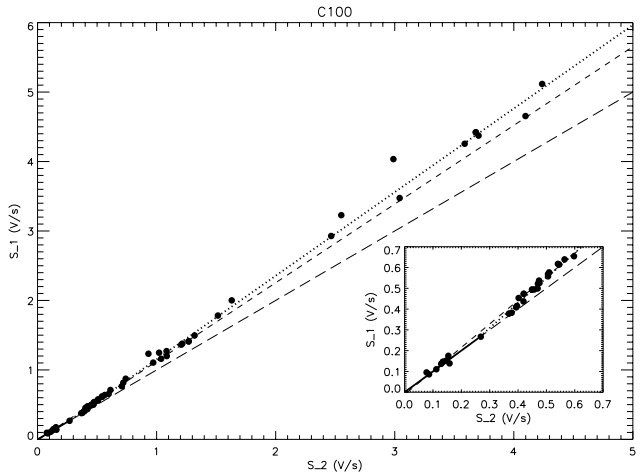

Figure 3. Reset interval relationship for signals obtained at RIs of 1 and 2 s (S_1 and S_2, respectively) for detector C100. Note that correlation 1:1 is reached for faint signal level. Solid and dotted lines correspond to the new fits for the two signal ranges considered. Short- and long-dashed lines refer to the current CALG fit and the correlation 1:1, respectively.

obtained at a certain RI, S_{RI}, to the reference RI = 1/4 s. A first version of this correction is implemented in PIA and can be activated at the SRD and SCP data processing levels.

2.2.1. Observations and data reduction

The complete set of dedicated observations designed to derive the RI correction for the P- and C- detectors was used. Data were processed with the ISOPHOT Interactive Analysis (PIA) version V9.1. The data reduction included ramp linearisation and deglitching. At the SRD level, dark signal subtraction was not performed, in contrary to analysis used in PIA. Our analysis is consistent with the general reduction scheme because the RI correction must be applied before dark signal subtraction.

2.2.2. Analysis and results

Firstly, signal relationships for consecutive RIs (1/32 and 1/16, 1/16 and 1/8, ... , 32 and 64 s) were analysed. We studied these correlations because signals of consecutive RIs have similar dynamical ranges and the number of pairs is higher than those for other possible combinations.

The measurements could not be fitted by a straight line only, but certain signal ranges had to be fitted individually and the linear fits forced to be connected at the border lines (see example in Fig. 3). A robust-line method was used to derive the parameters of the fits.

In order to shape the relationships not more than 3, 2, 2, 1 and 2 signal ranges for detectors C100, C200, P1, P2 and P3, respectively, were required. From the parameters of the adjacent pairs relationships it was possible to derive those ones for $S_{1/4}$ versus S_{RI} by a propagation method. In addition, the applicable signal ranges for each RI were computed.

Differences between the new and the previous RI corrections for P-detectors were noted. These are more significant for long reset intervals ($>$ 4 s) for which a 1:1 correlation is reached (as previously noted by del Burgo et al. 2001). Fig. 4 illustrates the impact of the new reset interval correction on the dark signal level for C100.

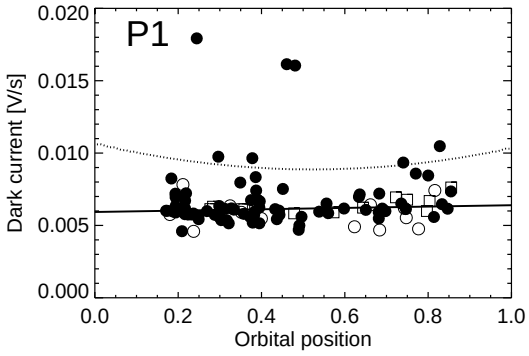

Figure 4. Dark signal versus orbital position for P1. The solid and dotted lines are the new and the previous fits, respectively. Different symbols correspond to reset intervals of 4 (squares), 8 (close circles) and 16 s (open circles).

For C100 most of the differences occur at faint signal level, where the present analysis shows a 1:1 correlation always for RIs $\geq$ 1/8 s (see Fig. 5, *top*). We also detect a different reset interval correction for the main diagonal (pixels 1, 5 and 9) and the rest of pixels for long RIs ($\geq$4 s). We created new pixel-dependent CALG files for the RI correction. For C200, no significant differences (see Fig. 5, *bottom*) are observed, but the residuals of the new fits are smaller than those in the previous version. previously noted, was inconsistent.

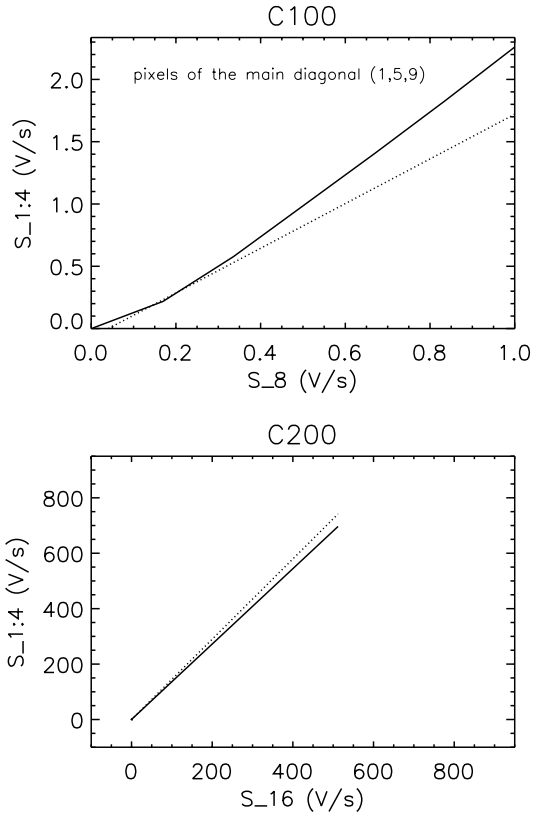

Figure 5. Top: Signal at RI=1/4 s versus Signal at RI=8 s for the pixels of main diagonal (1, 5, 9) of C100. Solid and dotted lines correspond to the new and previous RI fits, respectively. Note no pixel-dependence was reported for the previous fit and therefore this is the same for all pixels (Laureijs et al. 2001). Bottom: Signal at RI=1/4 s versus Signal at RI=16 s for C200. Solid and dotted lines as in top panel.

2.3. An empirical transient correction

After an illumination change, the output signal shows a systematic drift in time (transient behaviour), which asymptotically approximates to a stable level. The characteristic stabilisation time depends on the flux level, the flux jump and the illumination history. The transient correction is required to determine and inter-compare final signals from sky and FCS measurements, in particular, if they have different exposure times.

The usual way to deal with the transient problem is to fit the signal with an appropriate function (e.g., PIA drift modelling) or look for stability at the end of the measurement (e.g., PIA drift recognition). In this section an empirical correction method for the transient behaviour of ISOPHOT C- detectors is presented.

2.3.1. Data reduction

All staring measurements with integration times longer than 128 s independent of the target (e.g.: FCS or sky measurements) and of the filter were selected: 1140 for C100 and 1397 for C200. The sample comprises a wide signal range and allows us to perform a statistical transient correction.

For each pixel the shape of the transient curve is determined predominantly by the signal difference between consecutive measurements. Thus, big upward flux steps settle relatively quickly and downward steps take much longer to stabilize. The signal of the previous measurement with the same detector (or of the previous raster step in the case of a raster), S_{init}, was subtracted from the current signal in order to obtain the signal jump related to the flux step. or during a preceding observation on the same revolution. S_{init} was set to zero if the previous measurement was obtained more than 5 minutes before the measurement of interest.

2.3.2. Analysis and results

The correction proposed is a transformation between the signal measured after a certain integration time, S_t, and the reference signal S_{128} (for integration time of 128 s). Signals S_t were determined fitting the data streams between 0 and 128 s with a 5th order polynomial. The choice of S_{128} as reference signal was according to the fact that it was the usual length of the measurements for establishment of the FCS calibration. The relationship S_t-S_{128} was established for a few intermediate times, a grid of powers of 2 (t = 4, 8, 16, 32 and 64 s) was best adopted to the temporal behaviour of the drifts.

Fig. 5 shows the plots for one pixel of C100. The well defined relationship permitted for deriving a statistical correction. At t = 64 s, most of the pixels are stabilised and close to the asymptotical level. However, pixels 1 and 9 show already a slight departure from the linear relationship. At shorter integration times the signal loss rises significantly and varies from 10 to 30% in the signal range 1-5 V s^{-1} at t = 32 s depending on pixel number and up to 50% in the same signal range at t = 16 s.

The relationships between S_t and S_{128} for each pixel are well represented by the following model function:

$$S_t = S_{128}[1 - a_0(n,t)e^{-S_{128}/a_1(n,t)}S_{128}], \quad (1)$$

where a_0(n,t) and a_1(n,t) are the fitted parameters for each pixel n and integration time t.

Signal loss for any integration time was then interpolated from our data set of discrete times in the (time, signal) space. We used a logarithmic interpolation in time and a linear one in signal.

2.4. By-passing sky light

By-passing sky light must be taken into account for the derivation of the responsivity, because of the sky background was still shining into the instrument in the calibration mode. It is determined from cold FCS measurements. The heated FCS measurements must be corrected for this additive component.

We already presented a re-analysis of the dark signal behaviour of ISOPHOT (del Burgo et al. 2001). We have repeated such analysis using the new RI correction presented here and

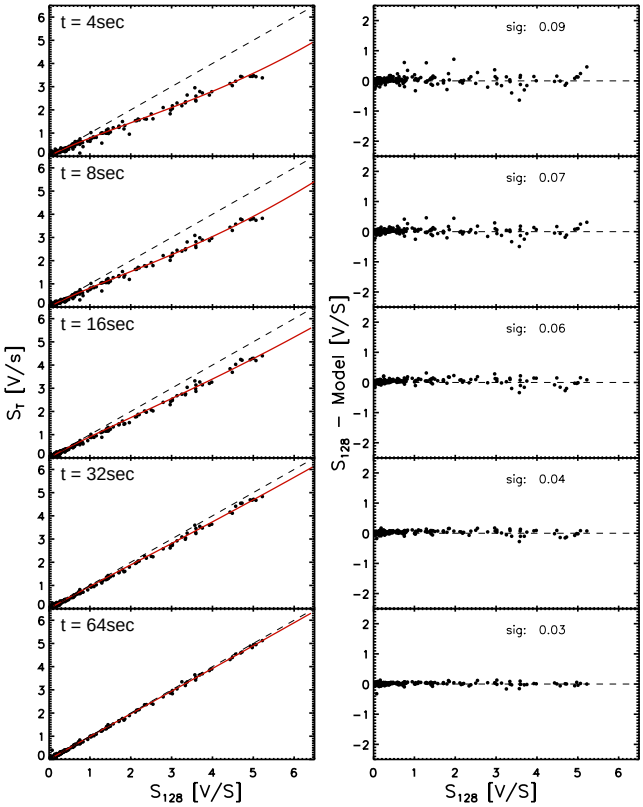

Figure 6. Left: Signals obtained after integration times of t = 4, 8, 16, 32 and 64 s versus the reference signal obtained after 128s. The curved line represents the fitted relationship used to derive the correction for signal loss at each time position. Right: Residuals after correction for the integration times (4, 8, 16, 32 and 64 s).

created new CALG files. Here we report for the first time an analysis of another additive instrumental component, the by-passing sky light, of the C-detectors. The by-passing sky light increases the FCS signal level and consequently contributes to overestimate the responsivity.

2.4.1. Data reduction

For each detector, all the sequences including cold FCS (FCS power = 0) and associated star and sky measurements were used. For each cold FCS, we selected the sky and star measurements with a close observing pointing ($\leq 1^{\circ}$), the same revolution and the same responsivity. Data were reduced with PIA V9.1 and new CALG files from SRD to SCP level: ramp linearization, deglitching, RI correction and dark signal subtraction. To determine the sky background, we only used the sky measurements for staring observations. For rasters, the sky background (for each pixel) was determined from the median of the 50% faintest measurements.

2.4.2. Results

We looked for correlations between the signal of the by-passing sky light and the signal of the sky background, the star and the total signal. A very clear dependence on the sky background signal is observed. Our analysis yields that the by-passing sky light amounts to 6% of the sky background for C200 for all 4 pixels. However, for C100, there is no pixel-uniformity. The by-passing sky light rises from ∼8% (pixels 1, 4, 7) over 10% (pixels 3, 9) to a maximum of 17% for pixel 6. No strong filter dependence seems to be present in any pixel.

3. Status and future plans

The results were reviewed in several internal calibration workshops and described in a set of calibration reports. In May 2002 the ISOPHOT Data Centre created a new version of PIA (V.11) which is under testing at the moment and will be made available to the scientific community. A paper presenting our results is in preparation.

Acknowledgements

CdB acknowledges the support by the EC TMR Network POE. Authors acknowledge the support from U. Klaas. PÁ thanks the support of the Hungarian Research Fund (Grant no. T037508) and of the Bolyai Fellowship.

References

del Burgo C., Ábrahám P., Klaas U., Héraudeau Ph., 2001, in: The Calibration Legacy of the ISO Mission, eds. L. Metcalfe et al., ESA-SP 481

Héraudeau Ph., Ábrahám P., del Burgo C., Klaas U., Kiss Cs., 2001, in: The Calibration Legacy of the ISO Mission, eds. L. Metcalfe et al., ESA-SP 481

Kessler M. F., Müller T. G., Arviset C., García-Lario P., Prusti T., 2000, The ISO Handbook Vol. I, ISO - Mission Overview, SAI-2000-035/Dc, Version.0

Laureijs, R. J., et al., 2002, The ISO Handbook Vol. IV.: PHT – The Imaging Photo-Polarimeter, SAI–99–069/Dc, Version 2.0

Lemke D., Klaas U., Abolins J., et al. 1996, A&A, 315, L64

Silverberg, R. F., et al. 1993, Proc. SPIE, 2019, 180

ACCURATE PHYSICAL MODEL FOR DIRECT MODELING OF POINT SOURCE TRANSIENTS FOR THE ISOCAM LW DETECTOR

Boris Fouks[1,2], Alain Coulais[2,3], and Jonathan Normand[2]

[1]Institute of Radio Engineering and Electronics of Russian Academy of Sciences,
11 Mokhovaya Str., GSP-3, Moscow, 103907, Russia
[2]Institut d'Astrophysique Spatiale (IAS), Batiment 121, Université Paris XI, 91 405 Orsay cedex - France
[3]LERMA, Observatoire de Paris, 61, Av. de l'Observatoire, 75 014 Paris - France

ABSTRACT

Under quasi-uniform illumination, the transient response of individual pixel of Si:Ga LW detector of ISOCAM detector is described with high accuracy by one of the Fouks' models, referred to Fouks-Schubert model. But this model fails its accuracy if the gradient of illumination between adjacent pixels is high.

We present here a general 3D physical model which allows to describe with a high accuracy most of the cases we encounter with ISOCAM. Besides the case of quasi-uniform illumination it is also applicable to the case of point sources. For the latter case, the narrower the PSF of the source, the higher the accuracy of the 3D model.

This model still uses the (β, λ) parameters which were used for the uniform illumination case. No supplementary parameters are required. But in the 3D case, where the exact topology of the detector array should be involved in the account, these two parameters describing the transient properties of each pixel are directly expressed through the parameters characterizing the technological quality of the detector bulk and its contacts. This fact provided the means to optimize future Si:Ga photodetectors.

We present here the direct model and also a preliminary inversion method. We discuss the limitations in the theory, the direct model and the correction method. This new physical model can now be used to reconsider the point source photometry and to remove all the artifact following observation of point sources in the raster maps. It is still important since the wavelengths of the ISOCAM LW detector ($\sim$5–18 μm) will not be covered by SIRTF and ASTRO-F.

Key words: ISO – CAM LW, Si:Ga, physical model, transient, crosstalk, point sources, photometry

1. INTRODUCTION

It has been shown that, at first order, the transient responses of all the Si:Ga detectors on-board ISO can be described by one model[1] coming form Fouks' theory (Fouks 1992; Fouks 1995) : Si:Ga detectors ISOPHT-S and ISOPHT-P (Fouks and Schubert 1995), ISOCAM-LW (Coulais and Abergel 2000) and ISOSWS-b2 (Kester 1999; Kester et al. 2002). This model is a simplification of the Fouks' theory assuming that
(1) the illumination of the pixel surface is uniform and
(2) the crosstalks between adjacent pixels in the same bulk essentially compensate each other.

It has been observed (Coulais and Abergel 2000; Coulais et al. 2000) for the LW detector of ISOCAM that the transient response for point sources cannot be described by this 1D model. Efforts to have a model for modeling the transients of point sources were engaged (Coulais et al. 2000; Coulais and Fouks 2002) with the goal to provide a high accuracy for the photometry of ISO sources (Blommaert 1998; Blommaert et al. 2000).

We report here the availability of such an accurate model. The 3D model is quickly described in Sect. 2, the correction method is explained in Sect. 3. We show examples in Sect. 4 and discussed few problems or limitations not mentioned in Sect. 3. Connections with physical properties are detailed in Sect. 5, and possible application to other Si:Ga photodetectors in Sect. 6.

2. THE DIRECT MODEL

The theory and the new full 3D physical model is extensively described in a technical note[2]. Validity ranges are discussed. Second order correction terms are given when the width of the PSF of the point sources becomes too large in comparison with the pixel size.

In order to test it and to apply it quickly to compare with the transient responses of CAM point sources, a simplified 2D model using symmetry properties of the detector array and of the sources was derived. Under uniform illumination, this 2D model was carefully compared with the 1D model and both give the same transients. Without any modification, with the same median $(\overline{\beta}, \overline{\lambda})$ parameters than under uniform illumination, the new model immediately gave the good shape for the transients of the sharpest point sources which are far from the transient response predicted by the 1D model (e.g. TDT 35600501, see Fig. 2).

It has been assumed that the profiles of point sources observed with the LW detector of ISOCAM have, at first order, a circular symmetry. This property was useful to simplify the model from 3D to 2D and to drastically reduce the estimated

[1] The well known so-called Fouks-Schubert model.

[2] This document, annexes and extra examples are available at : `http://www.ias.fr/PPERSO/acoulais/ISO/Sources/transients_sources.html`

computing time. We know this assumption of symmetry is not very exact for CAM (Okumura 1998; Okumura 2000), but (1) we need to use such a 1D profile in order to use the 2D model and
(2) the exact shape of the real profile is not well known (Okumura 1998; Okumura 2000) and
(3) the errors are not too large and other problems seem to be more critical (see below). On contrary, a good approximation with circular symmetry is available (Okumura 2000).

3. THE CORRECTION METHOD

Contrary to the 1D case (Coulais and Abergel 2000), no "trivial" and direct correction method can be derived from the equations of this new model. The problem is much more complicated than for the uniform case since we have to process at least the 3×3 pixels centered on the brightest pixel at the same time. In order to extensively check the model on real data, a dichotomic method was setup, to find one to three of the six parameters describing one configuration :

- (x, y) position, at scale much smaller than pixel size;
- J_0^b stabilized flux of the background before observing the source;
- J_1^b stabilized flux of the background during observing the source;
- J_1 stabilized flux of the source;
- σ full width at half maximum (FWHM) of the source (possible profiles are Gaussian or Bessel, see below).

Here we have strongly limited the capabilities of the the model since it can take into account a non-stabilized initial level and a non-uniform initial level, but we did not take into account these extra complications in the method.
We use the following notations: x^i means *initial* value of x, x^e *estimated* value of x, $\widetilde{x}$ *true* value of x.
Estimations for (x, y) and initialization of σ^i are made using 2D Gaussian fitting on each readout in a block, then the median values are used. In simulations, without or with noise, and for real data, this fitting works well. Nevertheless, we made two errors :
(1) a very small for (x^i, y^i) which are slightly shifted with respect to $(\widetilde{x}, \widetilde{y})$ depending on the position of the source on the pixel due to inadequate profiles and transient effects and
(2) a larger one for σ^i which is not close to $\widetilde{\sigma}$ because of modifications of the source profiles (in σ and in amplitude) during the transient.

The problem to find a good initialization (J_1^i, J_0^i, σ^i) is not simple because the transient response modifies σ and is strongly non-linear with J_0^b when J_0^b is close to zero. Furthermore, we can not derive J_1^i directly from data because of the transient but also because of effect of the PSF width.

Let's assume that we know with a high accuracy the J_0^b value. It has been checked in simulations that inside a given range (e.g. $\widetilde{\sigma} \pm 50\%$ and $\widetilde{J_1} \pm 50\%$, constant J_0, x and y) the criterion we used is convex with only one maximum. At large scale (real value $\pm50\%$), this 2D criteria (with J_1 and σ) has roughly a Gaussian shape with an anti-diagonal orientation. It indicates that we cannot go directly to the optimum with the dichotomy. On the contrary, it has been observed a good property when the estimated values (σ^e, J_1^e) are close (real values $\pm10\%$) to the true ones (σ^i, J_1^i) : the shape of the criteria becomes similar to a high elliptic Gaussian with axis aligned with σ and J_1. This fact ensures a fast convergence of the dichotomy in the vicinity of the optimum. Furthermore, this indicates that, after the processing of a significant number of sources with different combination of lenses and filters, we can tabulate the relationship between the real FWHM PSF $\widetilde{\sigma}$ and the estimated one σ^i during initialization, and concentrate only on J_1 the estimation.

During the dichotomy, we use several tests (sign of the difference between the estimations and the data, for the brightest pixel and four closest ones) to indicate simply in which direction we have to move. Because of approximation on the PSF shape, of possible problems due to the specific noise[3] in the transient response for point source, which is much higher than under uniform illumination (Coulais and Fouks 2002) and because we know that for a few number of cases the model is only a first order approximation, several criteria have been considered. It seems that the Least Square Criteria on the brightest pixel and its four closest pixels (i.e. without the four pixels in diagonal) is the best candidate. Because of the approximation due to the non-symmetrical PSF, we see that, with a Gaussian PSF, we make the largest errors for them, in comparison to the brightest one and the four closest ones. Furthermore, the diagonal pixels generally did not contribute a lot.
We are currently assuming that the unknown values are: J_0^b, J_1, σ.
σ is assumed unknown because :
(1) the width of the PSFs are changing during transient responses,
(2) we assume now a Gaussian PSF but the real PSFs are closer to the Bessel ones.
It is clear that for a given configuration (a lens and a filter) we should have a fixed value for σ in the future. Since we have processed only a limited number of sources, such shortcut can not be done now. But such tabulation will be very useful to speed up the correction method later. This model is also the way to reconsider on firm basis the computation of the FWHM of the PSF by removing the effects of transients in the FWHM estimation, and we expect a reduction of error bars for the FWHM with the help of this model.

For most of the sources (more than thirty sources) on which we have applied this correction method the adjustment was done with a good accuracy in 20 to 30 iterations. Depending on the number of readouts for which the transients are computed, the time for one iteration is $\sim$ 5–30 s. When the uncertainties for J_0 are high (e.g. when J_0 is close to zero, say, $J_0 \lesssim 5$ ADU)

[3] On pixels under high illumination gradients we have a particular noise with high amplitude in comparison to the noise measured under uniform illumination. This noise is strongly correlated between two adjacent pixels. This exchange of currents (crosstalk) between adjacent pixels reflects the satellite jitter.

or when J_0 is not uniform, we need about two times more iterations.

Since the model did not need to find *adhoc* parameters we are looking only for x, y, J_0, J_1, σ. For a well characterized configuration, J_0 and σ are well known, it is easy to find (x, y) at few percent based on a few readouts. Then we are looking for J_1 only ! Flux for sources observed with a small numbers of readouts can also be very well estimated; it has been confirmed by simulations and with datasets where we reduce the number of readouts.

4. EXAMPLES AND LIMITATIONS

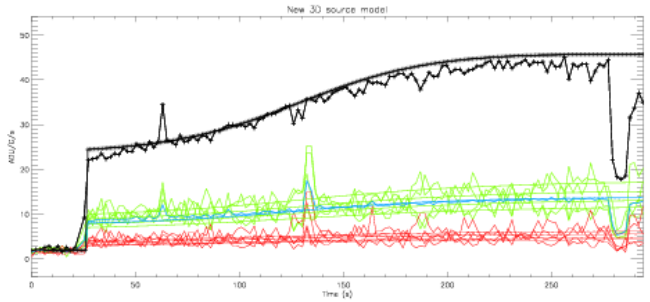

Figure 1. TDT 07803313 is typical for a quick observation for IR stars. Only a very limited time before the observation is available which may give problems to accurately determine whether the initial conditions are stabilized. In this case, the stabilization is good, and the illumination before the source observation is also well uniform. In this configuration (lens 1.5 arcsec and filter LW 6), the PSF width is small enough to ensure a good accuracy for the model.

Since the set-ups for the ground based tests and for the in-flight electrical set-ups are different, thus this results in different (β, λ) parameters (Coulais and Abergel 2002 and references therein). We have applied the model and the correction method only on in-flight data.

Up to now, not all the CAM configurations have been checked (10 filters LW 1–LW 10 and 4 lenses (1.5, 3, 6 and 12 ArcSec)) nor the full range for sources and backgrounds (before and during source observation). Nevertheless, about thirty sources have been successfully processed (in $\sim$ twenty five different TDTs). We give here three independent examples : on Fig. 1, a very simple case;
on Fig. 2, a case where the downward transient can be also studied and
the Fig. 3 shows one of the worst cases, with the second order correction term.

We say that the larger the PSF, the less accurate the 2D model. We are in the limit of validity for the model for the four CAM configurations giving the largest PSF : lens 1.5 ArcSec and filters LW 3, 9 ,10, 8. Nevertheless the 3×3 mean transients are in general in good agreement between model and data.

The physical reason of this difference is clear. Because of the topology of the CAM array (very long inter-contact distance when compared with the pixel size, ratio is 5:1) here it is essential the effect of the inter-pixel currents induced by very small radial fields. This idea, which clearly follows from the physics of the detector operation has been confirmed by the estimations of this effect in limiting cases and their comparison with experimental data. This effect is not considered yet in the used model, but can be taken into account in its following development.

This departure between model and data is clear especially for the overshoot for the brightest pixel during the upward transient. The second order term helps to improve the description the transient response for the brightest pixel. This term clearly improves the description of transients for these four configurations. We show a difficult example on Fig. 3.

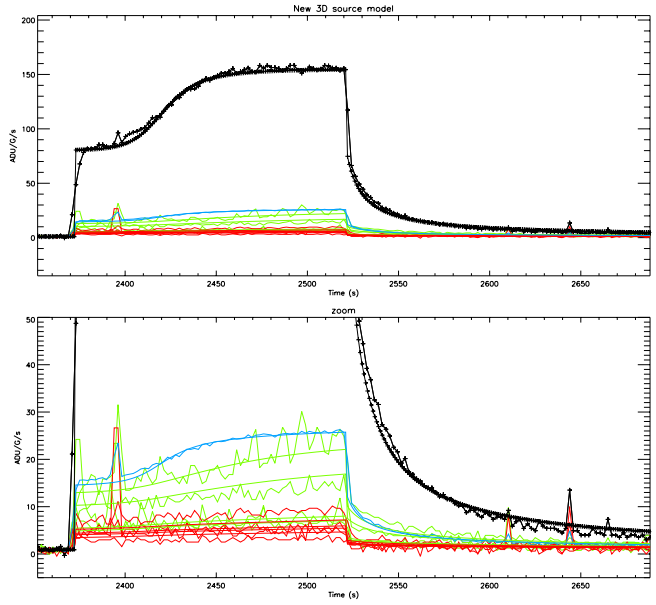

Figure 2. TDT 35600501 is very interesting to check different effects in the model because the same source is observed in the same configuration (Lens 3, Filter LW 2) by different pixels several times ($\sim$36 elementary observations in the same TDT with same background). Data and model are superimposed here for upward and downward transients. Only a fraction of readout gives the shift between data and model for the downward step. On the upper panel, we see the quasi-perfect agreement for the brightest pixel. On the lower panel, the change in Y-scale shown that, despite a good global agreement, we have to improve the agreement for time between 2370-2420. For all the tests reported in this note, we did not take into account the inter-pixel variations for the (β, λ) parameters. This TDT should be useful to study this dependence.

It has been mentioned several times that we still have troubles due to limited accuracies of the dark correction. It has been explained that the Fouks model allows to derive the absolute levels (see for ex. Coulais and Abergel 2002), unfortunately, only a very limited number of flux steps under uniform illumination can be processed (Coulais and Abergel 2000). From preliminary tests on point sources, it may be possible to use

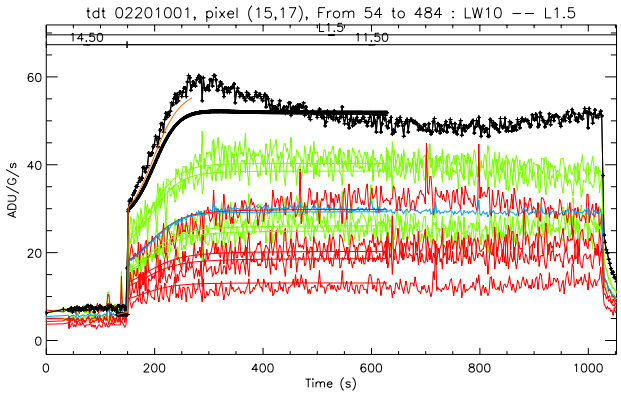

Figure 3. The combination of filter LW10 and lens 1.5 arcsec gives one of the four bad combinations for the model presented in this paper. In these cases, it is expected that the model under-estimated the real transient for the brightest pixel. This effect is described in the Fouks technical note. A second order correction term is computed, and is superimposed here (see the curve limited in range between T=150 and 275, in between the data and the model for the brightest pixel.) Furthermore, the study of this source is very complex because the illumination before the source is not uniform. It is easy to see when changing initial conditions J_0^b in the model how big are the change for the transient shape of brightest pixel. Despite all these problems, the overall responses are not too far from the real responses, and the 3×3 mean curves overlap.

this new model and experimental data of point sources to recover the accurate dark level when J_0 is close to zero and too noisy. Two interesting examples we have studied are sources in TDT 10801813 and 35600602. For the first one, the dispersion of the background before observing the source is very high. Transient correction allows to derive a estimation not only of this source but also of the mean background before the source.

As explained in Sect.3, we have written the model only in a 2D way, despite the new model is fully 3D. As a result, the profile of the source can be only a circular one. This simplification was done for simplicity shake and for testability. Nevertheless we are not sure now that the full 3D code gives a higher usefulness than the 2D one, since no simple inversion method can be applied to it. A large number of possible problems must be checked before working on the 3D model : dependence on the (x, y) values and onthe satellite jitter, on the PSF profile, on the limited accuracy of the dark level and on the non-uniform non-stabilized initial level (J_0).

5. RELATION WITH PHOTODETECTOR TECHNOLOGY

This 2D model still uses the (β, λ) parameters used for the 1D model for the uniform illumination case (Coulais and Abergel 2000). No supplementary parameters are required. These parameters are related for each pixel to the instantaneous jump (β) and the time constant (λ) The parameters (β, λ) can be converted into two physical parameters $(E_j, Gain)$ which are directly related to the quality of the contacts and the homogeneity of the bulk, respectively.

These parameters are connected to the detector quality from the technology point of view. Dispersion of these parameters through the array indicates poorly controlled technological processes. Theoretical limits are also known from the Fouks Theory. For ISOCAM (see description of (β, λ) maps in Coulais and Abergel 2000), we have found that
(1) the bulk quality of the matrix array is rather good and is well uniform, but
(2) the quality of contacts is not uniform and is far from theoretical limits.
Being closer to these limits should give a transient response up to five time faster. Nevertheless CAM detector is a good one since it is described by zero and first orders models from the Fouks theory over a large range of incoming flux, which allows a very accurate correction of its transient responses, despite a "small" instantaneous jump and a "long" time constant.

6. RE-USE FOR OTHER SI:GA PHOTODETECTORS

This model should be re-usable for any Si:Ga detector, when the electrical voltage is not too strong, in order to avoid extra non-linear effects. On-board ISO, the ISOSWS-b2 linear array, the ISOPHT-S (linear array) and ISOPHOT-P (single pixel) are Si:Ga detectors as well. But from our current understanding of the status of the processing of ISOSWS-b2, ISOPHT-S and ISOPHOT-P, the first priority for ISOSWS-b2 is to apply the model for non-linearity close to the avalanche breakdown (Kester et al. 2002) and for ISOPHT-S and ISOPHOT-P is to apply the correction method detailed in Coulais and Abergel 2000, assuming the two parameters (β, λ) are constant.

7. CONCLUSION

We are now able to model and correct with a high accuracy the transient response for point sources and under uniform illumination for the Si:Ga 32×32 array of ISOCAM's LW detector. The transient response of the mean value of the 3×3 pixels centered of the brightest one is described at percent level. The transient responsees of individual pixels are described at few percent level. Worst cases for individual pixels are for combination of lens 1.5 ArcSec and filters LW 3, 9, 10 and 8. One time again it has been proved (1) the power of such physical model and (2) the good quality of CAM detector array.

We are ready to provide this 2D model and to assist any scientist who would like to reconsider the ISOCAM point source photometry with the LW detector.

One time again, we mentioned that the Fouks theory was successful for all the Si:Ga but also for all the studied Ge:Ga on-board ISO with models described before ISO flight (Fouks 1992; Coulais et al. 2002). This theory should be useful for the photodetectors in preparation (SIRTF MIPS, Astro-F FIR and FTS, Herschel PACS) even if the theory must be transformed

into specific models adapted to the peculiarities of each detectors.

ACKNOWLEDGEMENTS

BF would like to express his gratitude to IAS, Orsay University and French CNRS for the invitations, financial support of his visits and nice conditions for the work. AC would like to thank BF for his patience and obstinacy to successfully complete this work. AC is grateful with French CNES, SaP CEA and IAS for financial supports during his long stay at IAS.

REFERENCES

Blommaert, J.: 1998, *ISOCAM photometry report*, Technical report, ESA Vilspa, Spain

Blommaert, J. A. D. L., Metcalfe, L., Altieri, B., Biviano, A., Okumura, K., Siebenmorgen, R., Guest, S., and Ott, S.: 2000, *Experimental Astronomy* **10**, 241

Coulais, A. and Abergel, A.: 2000, *Astron. Astrophys. Suppl. Ser.* **141**, 533

Coulais, A. and Abergel, A.: 2002, ESA SP-481, in press

Coulais, A. and Abergel, A.: 2002, this volume

Coulais, A., Abergel, A., and Fouks, B.: 2002, in Wolf, J., Farhoomand, J. and McCreight, C.R (eds.), *far-IR, sub-mm & mm detector technology workshop*, Vol. NASA/CP-211408

Coulais, A. and Fouks, B. I.: 2002, ESA SP-481, in press

Coulais, A., Fouks, B. I., Giovannelli, J.-F., Abergel, A., and Sée, J.: 2000, in M. Strojnik and B. Andresen (eds.), *Infrared Spaceborne Remote Sensing VIII*, Vol. 4131, pp 205–217, SPIE, San Diego, USA

Fouks, B. I.: 1992, in *ESA SP-356 Photon Detectors for Space Instrumentation*, pp 167–174

Fouks, B. I.: 1995, *Proceedings of SPIE* **2553**, 489

Fouks, B. I. and Schubert, J.: 1995, *Proceedings of SPIE* **2475**, 487

Kester, D.: 1999, *The impact of memory effects correction on SWS data*, Technical report, SRON, Netherlands

Kester, D., Fouks, B. I., and Lahuis, F.: 2002, ESA SP-481, in press

Okumura, K.: 1998, *ISOCAM PSF report*, Technical report, ESA, Vilspa

Okumura, K.: 2000, ESA SP-455

THE LARI METHOD FOR ISO-CAM/PHOT DATA REDUCTION AND ANALYSIS

Carlo Lari[1], Mattia Vaccari[2,3], Giulia Rodighiero[2], Dario Fadda[4], Carlotta Gruppioni[5,7], Francesca Pozzi[6], Alberto Franceschini[2], and Gianni Zamorani[7]

[1] Institute of Radio Astronomy, CNR, Via Gobetti 101, I-40122, Bologna, Italy
[2] Department of Astronomy, University of Padova, Vicolo dell'Osservatorio 5, I-35122, Padova, Italy
[3] CISAS "G. Colombo", University of Padova, Via Venezia 15, I-35131, Padova, Italy
[4] Instituto de Astrofisica de Canarias, Via Lactea S/N, E-38205, La Laguna, Tenerife, Spain
[5] Padova Astronomical Observatory, INAF, Vicolo dell'Osservatorio 2, I-35122, Padova, Italy
[6] Department of Astronomy, University of Bologna, Via Ranzani 1, I-40127, Bologna, Italy
[7] Bologna Astronomical Observatory, INAF, Via Ranzani 1, I-40127 Bologna, Italy

ABSTRACT

The techniques and software tools developed for the reduction and analysis of ISO-CAM/PHOT data with the LARI method are presented. The method, designed for the detection of faint sources in ISO raster observations, is based on the assumption of the existence of two different time scales in the detectors' transient behaviour, accounting either for fast or slow detectors' response.

The specifically developed IDL software includes: a reduction pipeline performing basic operations such as deglitching and background determination; the fitting procedures proper, modelling the time history of individual pixels and detecting any flux excess with respect to the local background ascribable to potential sources; mapping, source extraction and flux estimation procedures; simulation procedures allowing one to estimate the errors arising from different instrumental and reduction effects. Moreover, an easy-to-use graphical user interface allows one to quickly browse the data and carry out the substantial amount of interactive analysis required when the automatic fit fails and to check the reliability of detected sources.

This method provides source lists of great reliability and completeness and an outstanding photometric accuracy, particularly at low redundancy levels, where the reliability of ISO-CAM/PHOT source lists at moderately bright flux levels has been a long standing issue.

In this work a description of the techniques and of the software tools that have been developed is given, alongside with some highlights from the results obtained thanks to their application to different fields.

Key words: methods: data analysis – infrared: general – surveys – catalogues

1. INTRODUCTION

All data gathered by the ISO satellite, and particularly those from the two ISO cameras, ISO-CAM and ISO-PHOT, are very difficult to reduce, both due to the strong transient behaviour of the cryogenically cooled detectors (Coulais et al. 2000) and to the frequent and severe cosmic ray impacts yielding qualitatively different effects (common glitches, faders, dippers, dropouts and others, Claret et al. 1998).

While it was demonstrated that it is possible, at least to a certain extent, to satisfactorily describe the satellite's different detectors' behaviour adopting some physical model, the large number of readouts involved in raster observations and the peculiar nature and strength of noise patterns also require efficient and robust algorithms to be developed so as to make the actual data reduction undertaking feasible in a nearly-automatic way.

A number of data reduction methods has thus been developed and tested, mostly on ISO-CAM deep fields (e.g. the PRETI method by Starck et al. 1999 and the Triple Beam Switch method by Désert et al. 1999). Unfortunately, such methods proved useless for all ISO-PHOT data or on ISO-CAM shallower fields, leading to a high number of false detections and severe incompleteness. Besides, these methods suffered from the lack of an efficient way to interactively check the quality of the data reduction when needed.

The LARI method (first presented in Lari et al. 2001) has been developed to overcome these difficulties and provide a fully-interactive technique for the reduction and analysis of ISO-CAM/PHOT raster observations at all flux levels, particularly suited for the detection of faint sources and thus for the full exploitation of the scientific potential of the ISO archive.

2. THE MODEL

The LARI method describes the sequence of readings, or time history, of each pixel of CAM/PHOT detectors in terms of a mathematical model for the charge release towards the contacts. Such a model is based on the assumption of the existence, in each pixel, of two charge reservoirs, a short-lived one Q_b (breve) and a long-lived one Q_l (lunga), evolving independently with a different time constant and fed by both the photon flux and the cosmic rays. Such a model is fully conservative, and thus the observed signal S is related to the incident photon flux I and to the accumulated charges Q_b and Q_l by the

$$S = I - \frac{\mathrm{d}Q_{tot}}{\mathrm{d}t} = I - \frac{\mathrm{d}Q_b}{\mathrm{d}t} - \frac{\mathrm{d}Q_l}{\mathrm{d}t} \qquad (1)$$

where the evolution of these two quantities is governed by the same differential equation, albeit with a different efficiency e_i and time constant a_i

$$\frac{\mathrm{d}Q_i}{\mathrm{d}t} = e_i\, I - a_i\, Q_i^2 \quad \text{where} \quad i = b, l \qquad (2)$$

Proceedings of the Symposium *"Exploiting the ISO Data Archive - Infrared Astronomy in the Internet Age"*, 24–27 June 2002, Sigüenza, Spain (C. Gry, S. B. Peschke, J. Matagne et al. eds., ESA SP-511)

so that

$$S = (1 - e_b - e_l)\, I + a_b\, Q_b^2 + a_l\, Q_l^2 \quad (3)$$

The values of the parameters e_i and a_i are estimated from the data and are constant for a given detector, apart from the scaling of the a_i for the exposure time and the signal level, which is governed by the

$$a_i = \frac{t}{t_0} \sqrt{\frac{S}{S_0}}\, a_{i,0} \quad (4)$$

where $a_{i,0}$ is the value of a_i relative to a reference exposure time t_0 and signal level S_0. The model for the charge release, however, is exactly the same for CAM and PHOT detectors.

In practice, an additive offset signal attributable to thermal dark current (and thus not accounted for in CIA dark current subtraction) is added to both S and I in the equation above when it is estimated to be important, i.e. when the deepest dippers' depth exceeds 10% of the background level.

The glitches (i.e. the effects of cosmic ray impacts on time history) are identified through filtering of the time history and modelled as discontinuities in the charge release, leaving as free parameters the charges at the beginning of the time history and at the peaks of glitches.

Iteration of the fitting procedure is interrupted when either a satisfactory data-model rms deviation is achieved or the maximum number of allowed iterations is reached. In Fig. 1 it is shown how a successful fit is thus able to recover useful information (specifically, source fluxes) from otherwise troublesome parts of the pixel time history.

3. THE METHOD

The reduction pipeline consists of the following steps:

- PHOT ramps' linearization (following Rodighiero et al. 2001) and data smoothing (i.e. median averaging over a suitable number of readouts)
- Standard CIA/PIA `raster` structure and data-reduction-dedicated `liscio` structure building
- Dark current subtraction, global background (or stabilization) level estimation, bright sources' and glitches' identification
- Time history fitting procedure and interactive "repair" on fitting failures
- Interactive checks on sources detected in time history
- Flat-fielding, mapping, and source extraction (using DAOPHOT's `find`, particularly suited for the detection of point-like sources)
- Interactive checks on sources detected on maps and back-projected on pixels' time history
- Source flux autosimulation

The fitting procedure describes the time history of individual pixels according to the mathematical model seen in Section 2, allowing the determination of the breve and lunga charge levels, the local background and the flux excess ascribable to potential sources at any given observing time (i.e. readout).

The so-called autosimulation procedure for source flux estimation accounts for mapping effects in the determination of the flux of detected sources through the following steps:

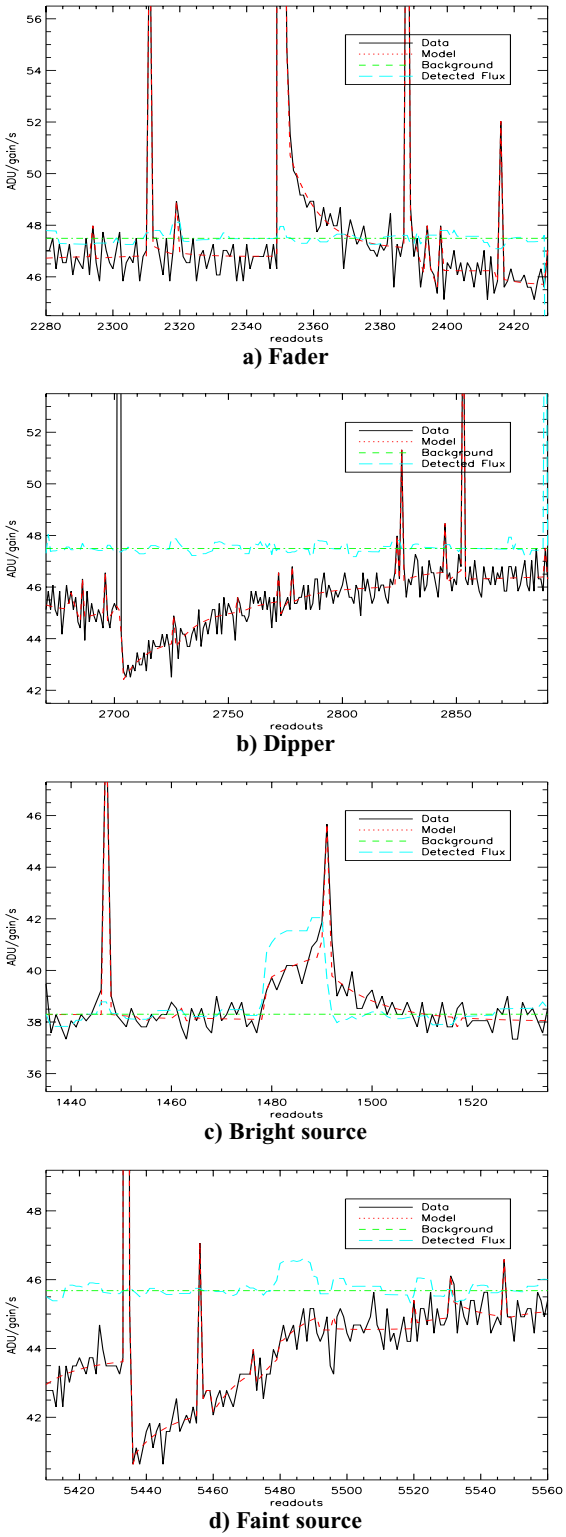

Figure 1. Different troublesome situations in ISO-CAM pixel time history: a) Recovery of stabilization level after a fader b) Recovery of stabilization level after a dipper c) Detection of a bright source hidden by a strong common glitch d) Faint source hidden by the recovery of the stabilization level after a dipper.

– First guess of source flux, based on its observed peak flux on the map
– Back-projection of source at the detected position on the time history
– Determination of theoretical peak flux on back-projected map
– Source flux correction based on observed / theoretical peak flux ratio

Other factors affecting the source flux estimates, namely those arising from the detectors' transient behaviour and possible systematic deviations from nominal sensitivities as well as from the reduction technique, are then evaluated through simulations and absolute flux calibration.

Once the reduction of all rasters of interest has been completed according to the recipe above, one can determine the necessary corrections to nominal astrometry (e.g. performing a cross-correlation analysis between the list of detected sources and a suitable external catalogue) and project nearby or repeated fields onto a common mosaic map, on which source extraction, autosimulation and interactive checks can furtherly be performed so as to increase the quality of the reduction through cross-checks of detected sources on different rasters, thus partly overcoming the severe problems at their boundaries.

4. THE SOFTWARE

The method relies on CIA (Ott et al. (2001)) and PIA (Gabriel and Acosta-Pulido (1999)) for basic raw data reading and manipulation and on home-made IDL routines for the data reduction proper. The massive necessary amount of interactive analysis is carried out with an easy-to-use graphical user interface, shown in Fig. 2, which allows any kind of "repair" which may be necessary.

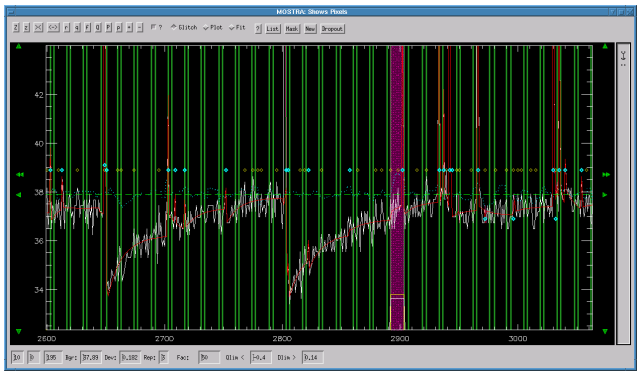

Figure 2. A screenshot of the IDL widget-based Graphical User Interface used to carry out interactive analysis.

5. RESULTS / WORK IN PROGRESS

All parameters indicating the goodness of the reduction (reliability, completeness, astrometric and photometric accuracy) are heavily dependent on the adopted observing parameters as well as on the thresholds chosen in the interactive "repair", and thus can only be evaluated through simulations.

While the catalogue resulting from the reduction of the first portion of ELAIS 15 μm data (Lari et al. 2001) are successfully being used for different purposes (see e.g. Gruppioni et al. 2002 and Matute et al. 2002), and the reduction of several different fields has already been completed, simulations and accurate photometric calibration are still being carried out, so that it is not presently possible to show detailed results. A list of the different projects being carried out includes:

– ELAIS 15 μm and 90 μm fields (Vaccari et al. 2002)
– Lockman Hole Shallow (LHS) and Deep (LHD) 15 μm and 90 μm fields (Fadda et al. 2002 and Rodighiero et al. 2002, see also Fig. 3)
– Hubble Deep Field North and South (HDFs) 7 μm and 15 μm fields
– A few nearby galaxy cluster 7 μm and 15 μm fields

while highlights from the expected results can thus be summarized:

– A catalogue of around 2000 15 μm sources in the 0.3-100 mJy flux range from LHS and ELAIS fields
– Catalogues of the uttermost quality in smaller, cosmologically relevant fields such as the LHD and the HDFs
– Flux-level-dependent photometric calibration based on predicted stellar IR fluxes (CAM) or on internal/external calibrators' reduction (PHOT)
– Unambiguous comparison of LARI fluxes with those obtained with different methods, e.g. on HDFs

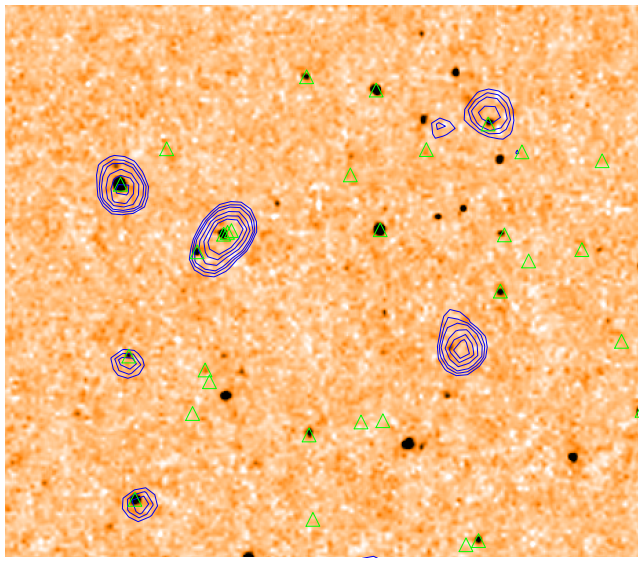

Figure 3. $15' \times 15'$ Lockman Hole 15 μm map, with overlaid 90 μm contours (blue lines) and radio sources (green triangles, from de Ruiter et al. 1997)

6. CONCLUSIONS

Originated as an answer to the problems posed by the ELAIS data reduction, the LARI method has evolved into a complete and well-tested system for ISO-CAM/PHOT data reduction and analysis, especially designed for the detection of faint sources and the interactive check of detected sources. Raster observations carried out with ISO-CAM LW detector at 7 and 15 μm and with ISO-PHOT C100 detector at 90 μm have been successfully reduced, while tests are foreseen to extend the method to other detectors.

Interactive by its very nature, the method both allows ISO-CAM/PHOT data reduction at all flux levels from scratch and to check the quality of any independent data reduction undertaking, thus leading to extremely reliable and complete source catalogues. It is thus believed that the LARI method can prove a very efficient tool in providing the community with an agreed-upon and substantial scientific return from the ISO archive.

ACKNOWLEDGEMENTS

This paper is based on observations with *ISO*, an ESA project, with instruments funded by ESA Member States (especially the PI countries: France, Germany, the Netherlands and the United Kingdom) and with participation of *ISAS* and *NASA*.

The *ISO-CAM* data presented in this paper was analysed using "CIA", a joint development by the ESA Astrophysics Division and the *ISO-CAM* Consortium. The *ISO-CAM* Consortium is led by the *ISO-CAM* PI, C. Cesarsky, Direction des Sciences de la Matiere, C.E.A., France.

PIA is a joint development by the ESA Astrophysics Division and the *ISO-PHOT* Consortium. The *ISO-PHOT* Consortium is led by the Max-Planck-Institut fuër Astronomie (MPIA), Heidelberg, Germany. Contributing *ISO-PHOT* Consortium institutes to the PIA development are: DIAS (Dublin Institute for advanced studies, Ireland) MPIK (Max-Planck-Institut fuër Kernphysik, Heidelberg, Germany), RAL (Rutherford Appleton Laboratory, Chilton, UK), AIP (Astronomisches Institut Potsdam, Germany), and MPIA.

This work was partly supported by the EC TMR Network POE programme (HPRN-CT-2000-00138).

REFERENCES

Claret A. et al. 1998, Glitch Effects in ISOCAM Detectors, ISO Technical Report

Coulais A. et al. 2000, Transient response of IR detectors used in space astronomy: what we have learned from ISO satellite, ISO Technical Report

Désert F. X. et al. 1999, A&A, 342, 363

Fadda D. et al. 2002, this volume

Gabriel C. and Acosta-Pulido J. A. 1999, ESA SP-427, 4

Gruppioni C. et al. 2002, MNRAS, accepted, astro-ph/0205173

Lari C. et al. 2001, MNRAS, 325, 1173

Matute I. et al. 2002, MNRAS, 332, L11

Ott S., Gastaud R., Ali B., Delaney M., Miville-Deschênes M.-A., Okumura K., Sauvage M., and Guest S. 2001, ASP Conf. Ser. 238, 170

Rodighiero G., Lari C. and Franceschini A. 2001, ESA SP-481

Rodighiero G. et al. 2002, this volume

de Ruiter H. R. et al. 1997, A&A, 319, 7

Starck J. L. et al. 1999, A&AS, 138, 365

Vaccari M. et al. 2002, this volume

PHOTOMETRIC INVESTIGATION OF THE ISOPHOT C100 MINIMAP MODE

Attila Moór[1], Péter Ábrahám[1], Csaba Kiss[1], Philippe Héraudeau[2], and Carlos del Burgo[2]

[1]Konkoly Observatory of the Hungarian Academy of Sciences, P.O.Box 67, H-1525 Budapest, Hungary
[2]Max-Planck-Institut für Astronomie, Königstuhl 17, D-69117 Heidelberg, Germany

ABSTRACT

As a possible concept to further improve the photometric accuracy of ISOPHOT we propose to concentrate on well-defined homogeneous data sets extracted from the Archive and carry out investigations focused on the specific calibration issues of the sample. The improvement of the photometric quality and that of the final error are monitored by selecting and evaluating secondary standards from the sample. In this contribution we describe the proposed general scheme and present – as an example – the analysis of 354 minimap observations of normal stars obtained at 60, 90 and 100 μm with the C100 detector. In the analysis we first determine measurement uncertainties characteristic of the OLP V10 data processing, and then check the improvements achieved by introducing the newly developed dynamic transient correction.

Key words: ISOPHOT - calibration: minimaps

1. INTRODUCTION

The release of the final version of the ISOPHOT (Lemke et al. 1996, Kessler et al. 1996) Off-Line Processing software (OLP V10) and the generation of the ISO Legacy Archive closed the main period of the ISOPHOT calibration. In that phase the calibration work focused on the main instrumental problems which affected several or all observing modes, and the correction algorithms developed were as general as possible in order to ease the software implementation. The photometric quality reached with the OLP is documented in the Scientific Validation Report (Klaas & Richards 2002) and in the ISOPHOT Calibration Accuracies Document (Klaas et al. 2002).

In a very general calibration approach, however, specific problems of individual observing modes (or submodes) may be overlooked or ignored. In order to further improve the photometric accuracy of ISOPHOT we propose to carry out more specific calibration investigations focusing on particular problems of well-defined homogeneous data sets, and to work out dedicated correction algorithm which are not necessarily applicable to other data sets. On the basis of ideas already discussed in several papers (Fajardo-Acosta et al. 1999, Laureijs et al. 2002) we propose the following general scheme for the analysis of a selected well-defined ISOPHOT observing mode or submode:

1. Collect all observations performed in the selected observing mode from the Archive;
2. Identify all objects which could be used as photometric standards;
3. Process the measurements of identified standard objects using the standard (OLP V10) data reduction method;
4. Search for a systematic trend in the (Measured-Predicted) residual flux densities;
5. Try to understand the reason behind the observed trend, invent new data processing methods to eliminate it and reprocess the data with the new methods;
6. Repeat Points 4-5 until all obvious reasons are eliminated;
7. Fit the remaining trend and work out an empirical formula to correct for the systematic discrepancies;
8. Document the new processing methods and the empirical fits;

Using the new reduction methods optimised for a selected mode we will re-analyse the entire data set of that observing mode. In this contribution we present the first results of the recalibration of the ISOPHOT C100 minimap mode in the framework of a joint project of Konkoly Observatory and the ISO Data Centre. The re-analysed data will be ingested into the ISO Archive. Sect. 2 describes the creation of a data base of 354 observations of normal stars. In Sect 3. we present the results of photometry obtained with OLP V10. In Sect 4. we summarize possibilities for improvements. Sect 5. demonstrates the effect of the dynamic transient correction. In Sect. 6 we discuss the different photometric behaviour of the individual pixels. Sect.7 summarizes the results of our investigation as well as the future plans.

2. DATA BASE OF NORMAL STARS

We searched the Archive and collected all minimap observations obtained with the C100 detector at 60, 90 and 100μm. In order to define a homogeneous sample we constrained the raster parameters to DM=DN=43–46″ and accepted only odd number of raster steps. This kind of minimaps were typically used for photometry of compact sources. Fortunately the sample turned to be rather homogeneous both in terms of observing time and read-out parameters.

The next step was to construct a data base which contained the possible photometric standards. We identified 354 measurements of 204 normal stars in a sample mainly originating from the Calibration Program and the 3 Vega programs (Decin et al.

Proceedings of the Symposium *"Exploiting the ISO Data Archive - Infrared Astronomy in the Internet Age"*,
24–27 June 2002, Sigüenza, Spain (C. Gry, S. B. Peschke, J. Matagne et al. eds., ESA SP-511)

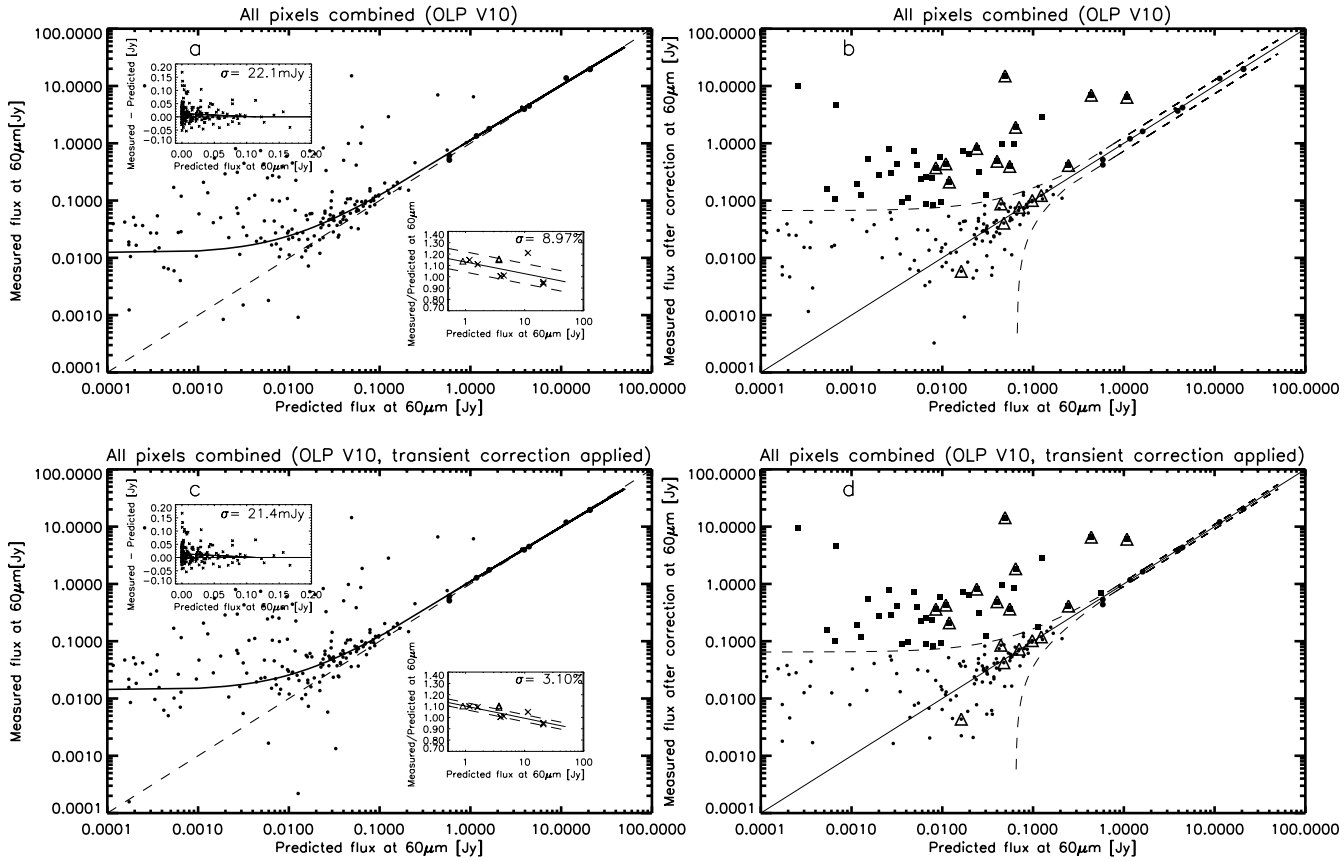

Figure 1. Measured vs. predicted flux at 60μm. 1a: original flux values with the correction curve following the main trends overplotted. The separate small windows present the relationship and the scatter around the trend at faint and bright level. 1b: the measured values are corrected for the systematic trend. Squares: stars with an excess above 3σ (Vega candidates). Triangles: Vega-type stars discovered by IRAS. Larger dots: FCS calibration stars. 1c-d : the same type of plot as Fig. 1a-b but we applied the dynamic transient correction.

2000, Habing et al. 2001 and Spangler et al. 2001). In order to use these stars as secondary standards we predicted their photospheric fluxes at far-infrared wavelengths. For this purpose we collected K (or V, when K was not available) magnitudes and B-V colour indices for the stars and derived relationships between the K-[25] and B-V indices where [25] is the magnitude at 25μm. The relationships were based and tested on a collection of stellar models produced by M. Cohen and P. Hammersley (available on the ISO homepage). Then flux densities in other filters were derived by multiplying the 25μm flux density by the F_λ / F_{25} infrared colour, which is itself a weak function of B-V. The accuracy of the prediction at 25μm from K magnitude is about 3%, from the V magnitude about 8%. Near infrared data were taken from the ISO Ground Based Preparatory program (GBPP, Jourdain de Muizon & Habing 1992).

3. PHOTOMETRY WITH OLP V10

According to the scheme drafted in Sect.1 we reduced the measurements of the normal stars. The data were processed in batch mode using PIA V9.1 with calibration (CalG) files compatible to OLP V10. Drift recognition was applied. To extract fluxes from minimap observations, we used the PCASPHT method (Kiss & Klaas 2000). This method is used at the ISOPHOT Data Centre (Heidelberg) and is implemented in OLP V10. It is based on the following principles:

- determine fluxes from the data stream of each individual pixel rather than creating a map;
- do not flat-field the pixels;
- assume a constant background;
- combine the fluxes obtained from the 9 detector pixels by using a robust average technique.

In Fig. 1a we display the results of the 60μm observations vs. the predicted fluxes of the stars. Systematic deviations from the models are observed at both faint and bright levels (see the two separate small windows). The thick line corresponds to a fit to the main trend. The measurement scatter around the fit is 22.1 mJy at low level and 8.97% at bright level. In the present analysis we adopt this scatter as an average error bar which we assign to all observations. The slow decrease of the measured/predicted ratio at high level might be due to slight inaccuracies of the FCS heating power curve. The offset-like deviation around zero is very likely related to the signal drift in the

minimap observation. Since there is no way to correct for these effects within the framework of OLP V10 we use the fitted line for an empirical photometric correction. In Fig. 1, panel b, we present the flux values after correction for the systematic trend. The dashed line is the $\pm 3\sigma$ level. Stars with excess above this threshold are plotted by squares. These stars, which constitute about 20% of the whole sample, may be surrounded by circumstellar dust (Vega phenomenon) and are analysed in a separate article (see Ábrahám et al. 2002). The Vega-type stars which were discovered by IRAS are denoted by triangles. The typical scatter values for the observations at 60, 90 and $100\ \mu$m are presented in Tab. 1. In the case of $100\ \mu$m data, our correction was based on 21 measurements of HR7310, therefore we give only one dispersion value.

4. HOW TO IMPROVE THE PHOTOMETRY?

There are several calibration issues which may play a role in the minimap photometry:

1. Improve ERD $\rightarrow$ AAP data reduction
   - Better de-glitching methods;
   - Transient correction within each raster position;
   - Drift correction (slow baseline variation which causes error in the background determination);
   - How to combine the two FCS measurements performed before and after the minimap?;
   - Subtraction of the by-passing skylight from FCS measurements (del Burgo et al. 2002).
2. Improve point source flux extraction
   - Better background determination, optimal selection of raster positions used as background;
   - Refinement of the FCS calibration curve;
   - Methods the combine the photometry of the nine pixels;

The items listed above may have different impact on the final photometry. In the following we test one of them, the transient correction within each raster position (see del Burgo et al. 2002).

5. PHOTOMETRY WITH OLP V10 + DYNAMIC TRANSIENT CORRECTION

A new transient correction algorithm, not implemented in OLP V10, was recently developed at MPIA and is available as IDL code. This new method fits the temporal signal evolution within a measurement on the basis of fits to a library of signal dependent transient curves and predicts the signal at t = 128s (for details see del Burgo et al. 2002). We processed the signals to SRD level as in Sect. 3, applied the transient correction by running the IDL code and then continued with the processing to AAP.

In Fig. 1, panels c and d, we present the transient corrected data of the observations at $60\ \mu$m when the nine pixels are combined. The standard deviation of the measurements at bright level shows remarkable decrease (9% $\rightarrow$ 3%). At the faint level the measurement error is practically unchanged (21.4 mJy). As we can seen in Tab. 1. the dynamic transient correction could not change noticeably the accuracy of the measurements at 90 and $100\ \mu$m. This phenomenon is due to the property of the dynamic transient correction, which has a forcible effect in the signal range of 1 - 5 V/s (del Burgo et al. 2002) and in the case of these wavelengths fewer measurement of stars fall in this signal range.

The transient correction did not cancel the systematic deviations from the predictions (see the two separate small windows in Fig. 1c). The remaining trend at high level is probably due to slight inaccuracies of the FCS heating power curve. The offset-like deviation around zero is very likely related to the signal drift in the minimap observation. As a future step correction algorithms for these two phenomena will be worked out. The effect of these corrections will be measured in a similar way as in the case of the transient correction, i.e. by changes in the final photometry. Should a remaining trend still be present an empirical fit and correction would be applied. Then all other non-stellar minimap observations can be processed.

6. PHOTOMETRY WITH INDIVIDUAL PIXELS

So far we discussed results obtained by combining the fluxes from the nine detector pixels. The investigation of the characteristics of the individual pixels, however, may also be interesting because it reveals the different photometric quality of the pixels. Moreover the correction curves per pixel can be used to evaluate other than minimap observations (e.g. irregularly sampled maps) where the photometry relies on the central pixel, Pix. 5 only. The results, summarized in Tab. 1, clearly show that the behaviour of the nine pixels are different. Unfortunately the central pixel, which plays a crucial role in other observing modes is not particularly good. The effect of transient correction is most visible at high flux level where it reduces the scatter around the main trend, especially in pixels 1, 5, 9.

7. CONCLUSIONS AND FUTURE PLANS

In this contribution we present a possible concept to improve further the photometric accuracy of ISOPHOT data. The basic idea is to concentrate on well-defined homogeneous data sets extracted from the Archive and carry out investigations focused on the specific calibration issues of the sample. The improvement of the photometric quality and that of the final error are monitored by selecting and evaluating secondary standards from the sample. The proposed general scheme is described in the text.

In order to demonstrate the concept we collected all regular minimap observations from the Archive. The 204 normal stars in the sample were selected as secondary standards and their 354 measurements were used to test the OLP V10 photometry

Table 1. Standard deviations of the observations from the main trend at 60, 90 and $100\ \mu m$ *using OLP V10 without/with dynamic transient correction. At faint level the sigma values are expressed in mJy while at bright end in percentages of the predicted flux.*

	OLP10					OLP10 and dyn. transient correction				
	σ_{60}^{faint}	σ_{60}^{bright}	σ_{90}^{faint}	σ_{90}^{bright}	σ_{100}^{faint}	σ_{60}^{faint}	σ_{60}^{bright}	σ_{90}^{faint}	σ_{90}^{bright}	σ_{100}^{faint}
	[mJy]	[%]	[mJy]	[%]	[mJy]	[mJy]	[%]	[mJy]	[%]	[mJy]
Combined pixels	22.2	8.97	20.1	4.87	18.6	21.5	3.1	19.4	5.3	17.9
Pixel 1	67.8	14.26	69.1	15.28	59.2	59.1	9.98	72.2	7.69	58.9
Pixel 2	57.1	8.78	45.8	7.3	42.9	56.8	6.37	46.2	9.75	41.1
Pixel 3	56.0	8.80	65.7	10.18	64.5	59.4	5.02	62.5	9.02	63.2
Pixel 4	67.2	4.18	55.5	7.03	54.2	67.9	4.35	57.8	8.88	50.9
Pixel 5	75.5	17.26	92.4	11.48	90.6	71.7	6.94	90.9	6.01	85.9
Pixel 6	102.2	10.62	75.7	17.28	173.1	105.5	9.45	77.6	16.05	170.0
Pixel 7	66.6	8.24	72.2	4.0	37.5	68.0	2.07	84.7	7.07	36.5
Pixel 8	38.1	14.81	44.2	5.75	44.7	38.0	5.91	44.0	4.27	42.2
Pixel 9	67.3	20.24	85.0	16.8	62.2	65.2	9.99	85.4	5.31	60.8

as well as the effect of the dynamic transient correction. With OLP V10 processing systematic deviations from the predicted fluxes became obvious. With the transient correction the trends remain unchanged but the error at bright level was significantly decreased.

The remaining trend in the residuals is probably due to drift effect within the minimaps as well as to slight inaccuracies in the FCS power curve. As a next step we plan to derive corrections for these two effects. We will also investigate the possibility to create individual, rather than average, error bars for the photometry of the stars. After processing all minimap observations the re-analyzed data will be ingested to the ISO Archive in the framework of the joint project of the Konkoly Observatory and the ISO Data Centre.

ACKNOWLEDGEMENTS

This work was partly supported by the Hungarian Research Fund (no. T037508). P.Á. thanks the support of the Bolyai Fellowship.

REFERENCES

Ábrahám P., Moór A., Kiss Cs., Héraudeau P., del Burgo C., 2002, this volume

Fajardo-Acosta S.B., Stencel R.E., Backman D.E., Thankur N., 1999, ApJ 520, 251

del Burgo C., Héraudeau P., Ábrahám P., 2002, this volume

Decin G., Dominik C., Malfait K., Mayor M., Waelkens C., 2000, A&A 357, 533

Habing H. J., Dominik C., Jourdain de Muizon, M., Laureijs R. J., Kessler M. F., Leech K., Metcalfe L., Salama A., Siebenmorgen R., Trams N., Bouchet P., 2001, A&A 365, 545

Kessler M.F., et al., 1996, A&A 315, L27

Kiss Cs., Klaas U., "General Re-validation of Point Source Photometry from PHT22 Mini-Maps", Internal calibration report, 17 May 2000

Klaas U., Ábrahám P., Laureijs R.J., Radovich M., Schulz B., Wilke K., 2002, ISOPHOT Calibration Accuracies Document

Klaas U., Richards P., 2002, Report on the Scientific Validation of PHT OLP Version 10.0

Laureijs R.J., Jourdain de Muizon M., Leech K., Siebenmorgen R., Dominik C., Habing H. J., Trams N., Kessler M. F., 2002, A&A 387, 285

Lemke D., et al., 1996, A&A 315, L64

Jourdain de Muizon, M., Habing H. J., 1992, Infrared Astronomy with ISO, Proceedings of a Workshop held in Les Houches, France Editors, Th. Encrenaz, M.F. Kessler, P. 129

Spangler C., Sargent A. I., Silverstone M. D., Becklin E. E., Zuckerman B., 2001, ApJ 555, 932

DEVELOPMENT OF THE ISOPHOT PIPELINE DURING THE ACTIVE ARCHIVE PHASE

Philip J. Richards[1] **and Ulrich Klaas**[2]

[1]CLRC, Rutherford Appleton Laboratory, Chilton, DIDCOT, OXON, OX11 0QX, UK
[2]Max-Planck-Institut für Astronomie, Königstuhl 17, 69117 Heidelberg, Germany

ABSTRACT

The development of the ISOPHOT pipeline has continued at the UKIDC beyond V10 used to generate the ISO Data Archive (IDA). A re-processing of selected subsets of ISOPHOT observations has been carried out for bulk ingestion into the IDA. These include all chopped PHT-S observations and the mini-map observations with the PHT-C arrays. The improvements to the algorithms are described and some results showing the enhancements to the data products are presented.

Key words: astronomical data bases:ISO Data Archive – methods:data analysis – infrared:stars,galaxies

1. INTRODUCTION

The development of the ISOPHOT pipeline has progressed in parallel with the calibration of the instrument and the quality of the data products has improved significantly since the end of ISO operations (Richards et al. 2002). The ISOPHOT component of the ISO Data Archive (IDA) contains data products, $\sim 90\%$ of which have been scientifically validated and a large proportion can be used with little or no further reduction for current astronomy research (Klaas et al. 2002).

Nevertheless, the IDA reflects the current state of the calibration and data processing at the beginning of 2001. In the meantime further progress has been made with our understanding of the detectors, their calibration and the data processing algorithms. Some of these developments lend themselves to automatic data processing and have been implemented in the ISOPHOT pipeline which is currently being supported at the UKIDC (as version PHTRP001). These developments have yielded improvements in data products for two large parts of the ISOPHOT database: the chopped PHT-S observations and the PHT-C mini-maps, which together represent $\sim 8\%$ of the complete database.

A brief description is given of the algorithms and some of the results are presented in comparison with models and the IDA products.

2. PHT-S CHOPPED SPECTROSCOPY

2.1. METHOD

The chopped PHT-S spectra in the IDA were produced using ramp deglitching and fitting to determine the on and off source signals (in V/sec) (Laureijs et al. 2002). However, experience with the data processing of chopped photometric measurements using the PHT-P and PHT-C detectors, where the number of readouts per integration ramp and the number of ramps per chopper pointing (plateau) are small compared to staring observations, has shown that alternative algorithms are more effective in removing glitches from radiation hits (Ábrahám et al. 2002). Rather than determining the source signal from the average of the signals obtained by fitting slopes to the ramps, the pair-wise difference signals (i.e. signals derived from adjacent detector readouts) were accumulated from all the ramps on a chopper plateau from which an outlier-resistant average was determined (using an implementation of an IDL procedure from the Freudenreich AstroContrib Library). Having determined the average signal in this way for a chopper plateau, the processing of the chopper plateau averages is the same as for OLP V10 as described in the ISO Handbook (Laureijs et al. 2002).

2.2. RESULTS

A detailed comparison of 25 observations with the Auto-Analysis results from the IDA (OLP V10, Klaas & Richards 2002) and model spectra has shown that the introduction of the outlier-resistant mean of the pair-wise differences has resulted in smoother continuum spectra. For calibration stars, the spectra are closer to the model spectra and for the galaxy spectra, with ground based spectra for comparison, the agreement is better and faint lines (PAH features and atomic lines) are more prominent. To demonstrate the improvements in the products, some specific examples from the validation of the processing are described below.

HR 6817 is one of two stars used to establish the Relative Spectral Response Function (RSRF) for chopped PHT-S measurements. In Fig. 1, the top spectrum is the reprocessed spectrum (labelled PHTRP001) from an observation executed in triangular chopped mode, which shows excellent agreement with the flux model (Hammersley et al. 1998). For comparison the IDA spectrum (OLP 10) is shown below, which shows a slight kink in the spectrum at $\sim 3\mu$m that does not appear in the PHTRP001 spectrum. The lower plot shows the deviation of the reprocessed spectrum from the model, the consistency with the model is $< 10\%$ absolute.

NGC 1068 is the brightest galaxy observed in this observing mode and the PHT-SS spectrum (2-5μm) is above the sen-

Proceedings of the Symposium *"Exploiting the ISO Data Archive - Infrared Astronomy in the Internet Age"*, 24–27 June 2002, Sigüenza, Spain (C. Gry, S. B. Peschke, J. Matagne et al. eds., ESA SP-511)

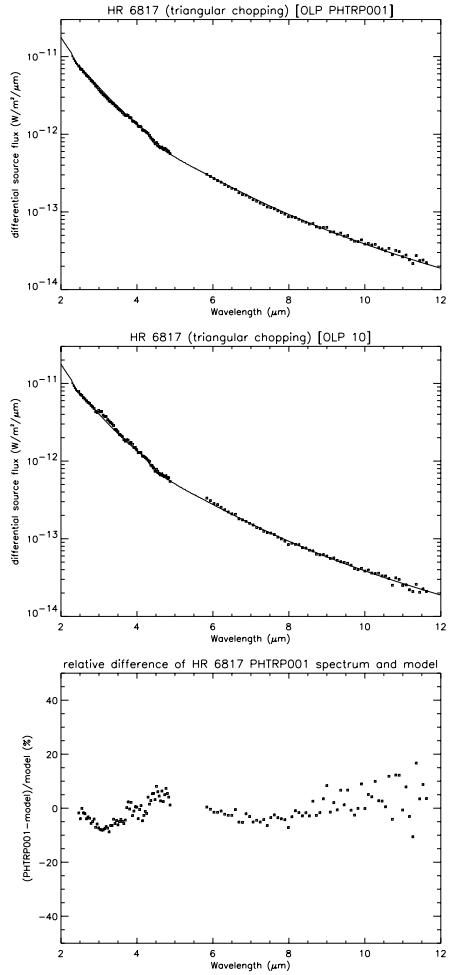

Figure 1. Comparison of the spectrum of HR 6817 obtained in PHT-S triangular chopped mode with the flux model by Hammersley et al. (1998). PHTRP001 spectrum (upper panel), OLP 10 spectrum (middle panel), relative difference of PHTRP001 to the model (lower panel).

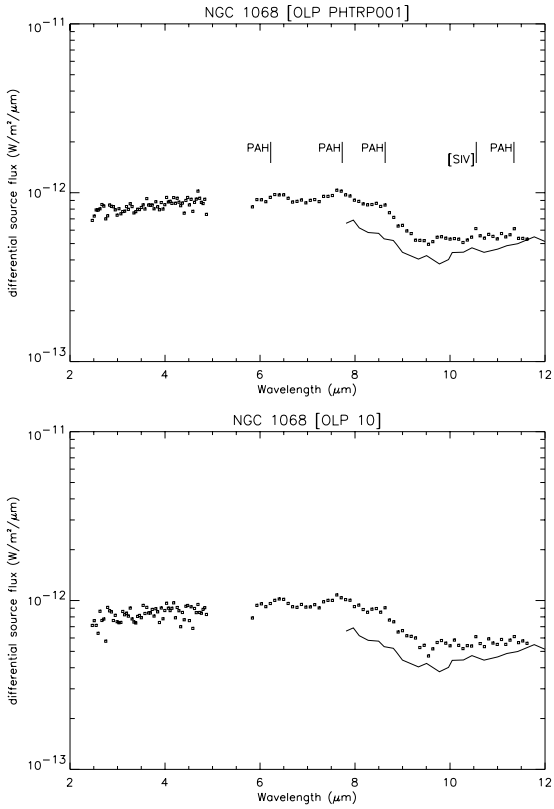

Figure 2. Comparison of the spectrum of NGC 1068 obtained in rectangular chopped mode (dots) with ground-based 8 – 13μm spectroscopy (solid line) by Roche et al. (1991) for both PHTRP001 (upper panel) and OLP 10 (lower panel).

sitivity limit ($\sim$ 7x10^{-14}W$m^{-2}\mu m^{-1}$). In Fig. 2, the PHTRP001 spectrum (top) is smoother than the OLP 10 spectrum (bottom) and there is very good agreement with ground based observations (solid line - note that these measurements were made with a smaller aperture than PHT-S, Roche et al. 1991). The smoother spectrum makes the weak 6.2, 7.7 and 8.6μm PAH features stand out. Also the line at 10.5μm ([SIV]) and the 11.3μm PAH feature now appear clearly above the continuum.

For the galaxy NGC 5506, the emission in the PHT-SS part is close to the detection limit. The PHTRP001 spectrum in the PHT-SL part (Fig. 3 (top)), showing strong silicate absorption, is again smoother than the OLP 10 spectrum. The weak PAH features at 6.2, 7.7 and 11.3μm can now be clearly identified above the continuum and also a, previously obscured, faint 8.6μm feature can be seen in the slope of the silicate feature. The red shifted [SIV] line at 10.6μm is clearly identified, as in the ground-based 8 – 13μm spectrum, and the red shifted [ArII] and [ArIII] lines are now in evidence around 7 and 9μm respectively.

3. PHT-C MINI-MAPS

3.1. METHOD

The PHT mini-map observing mode using the PHT-C arrays has enabled accurate photometry to be performed on faint sources down to $\sim$ 50mJy with the C100 array and $\sim$ 100mJy with the C200 array, using a method developed by Kiss (Klaas et al. 2000) which processed the pipeline PCAS products from these observations. This is a considerable improvement in the photometric accuracy compared to that obtained from aperture photometry on the PGAI image products and has been implemented in the PHTRP001 version of the pipeline.

In a mini-map raster observation, each pixel of the PHT-C array points at the source and surrounding background positions. The assumption is made that the measured flux per pixel is the sum of a fraction of the source seen by the pixel (determined from the footprint) plus a (constant) background flux. For each pixel, a linear fit is made to the observed flux at a raster position as a function of footprint fraction for that raster position. This provides an estimate of the source flux (the slope) and the background (the offset). The average values for the

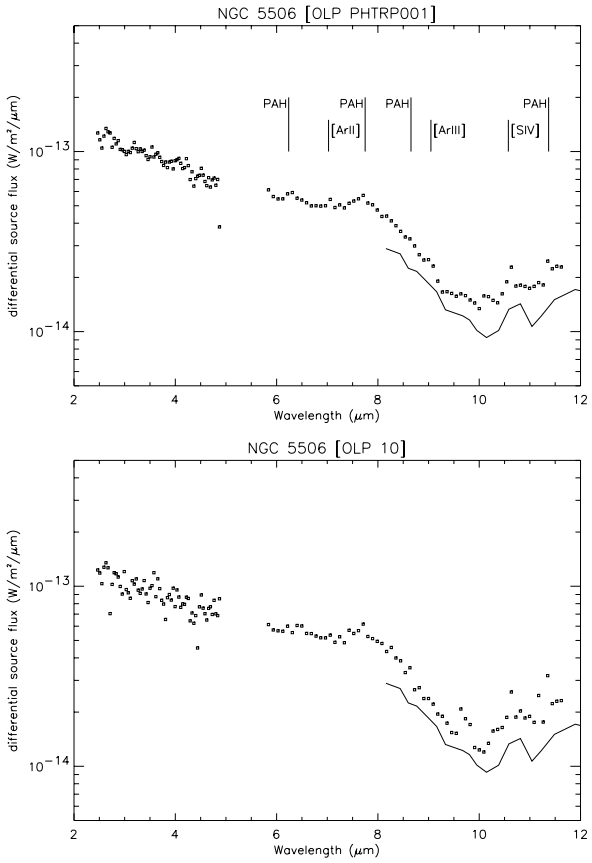

Figure 3. Comparison of the spectrum of NGC 5506 obtained in rectangular chopped mode (dots) with ground-based 8 – 13μm spectroscopy (solid line) by Roche et al. 1991 for both PHTRP001 (upper panel) and OLP 10 (lower panel).

source flux and background over all pixels are then determined using a bi-weight mean. The resulting source flux density and background surface brightness are stored as keywords in the PGAI header.

The fraction of the source seen by a pixel for a given offset relative to the centre of the source has been determined by Laureijs (1999). At present these footprint fractions only exist for offsets given by the centre of the pixels relative to the centre of the array, that is fractions do not exist for pixels centred a fraction of a pixel width from the centre. Therefore mini-maps have only been reprocessed if steps between raster pointings are a pixel width, that is $46''$ for C100 and $92''$ for C200. Also the footprint fractions are those derived assuming a point source, so, to obtain the actual flux density for an extended source, the footprint fractions would have to be modified accordingly.

3.2. Results

Mini-map observations of the calibration star HR 1654 were executed for all C100 filters and three out of the five C200 filters. Fig. 4 shows a comparison between the photometry from the processing with the Kiss IDL procedures used to evaluate the IDA (OLP 10) products (top) and the flux densities from the pipeline algorithm (PHTRP001) in the PGAI headers (bottom). The model spectrum of Cohen et al. (1996) is also shown as a solid line. The numerical values are also given in Table 1. (Note that all flux densities have been colour corrected assuming a black body with T = 4000 K.)

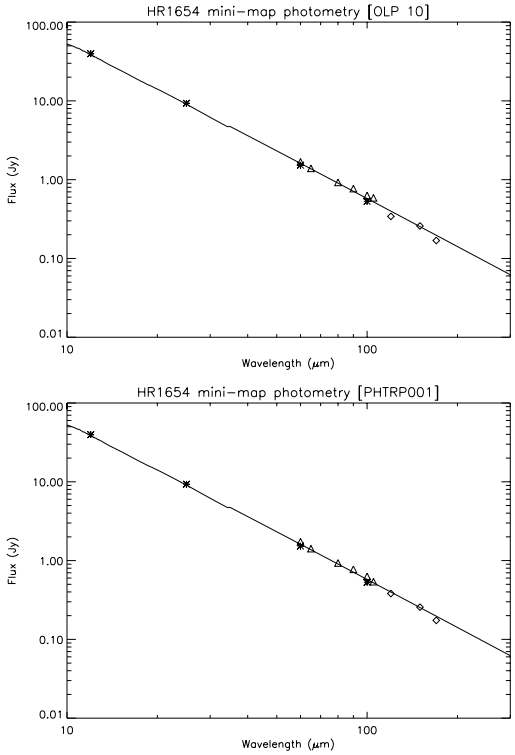

Figure 4. Comparison of PHT-C mini-map photometry with the model spectrum (plus extension out to 300 μm) of HR 1654 provided by M. Cohen and with IRAS photometry for OLP 10 (upper panel) and PHTRP001 (lower panel). All photometric points are color corrected for a 4000 K BB. The meaning of the symbols is the following: solid line: model, asterisk: IRAS, triangle: PHT-C100 (P22 AOT), diamond: PHT-C200 (P22 AOT).

From Table 1 it can be seen that the C100 absolute photometric accuracy for the pipeline (PHTRP001) products are $< 10\,\%$ for all filters and $< 12\,\%$ for the three C200 filters, being $< 5\,\%$ at 120 and 150μm.

The implementation in the ISOPHOT pipeline assumes a point source, so if the source is extended the footprint factors will not apply. HD 216956 (Formalhaut) is a star with extended emission in the FIR associated with a circumstellar disk. The top row (C1) in Table 2 gives the 60μm flux densities from the IDA (OLP 10) and the PHTRP001 products which are in very good agreement, but well below the IRAS and model flux densities. However, if a $22''$ Gaussian footprint is used instead to account for the Formalhaut disk, the 60μm flux increases to the value in row C1e which is more consistent with the IRAS photometry.

Table 1. HR1654 - comparison of the flux densities from the IDA PCAS product (OLP 10) and the PHTRP001 (RP001) processing. Δ gives the relative deviation from the model in %.

Det	cwl (μm)	OLP 10	RP001	Model	Δ (RP001)
C1	60.0	1.682	1.736	1.610	7.82
C1	65.0	1.391	1.417	1.372	3.28
C1	80.0	0.924	0.932	0.903	3.18
C1	90.0	0.770	0.774	0.713	8.66
C1	100.0	0.630	0.629	0.576	9.22
C1	105.0	0.588	0.540	0.522	3.40
C2	120.0	0.342	0.382	0.399	-4.26
C2	150.0	0.258	0.257	0.254	1.09
C2	170.0	0.169	0.174	0.197	-11.61

Table 2. HD216956 - comparison of the flux densities from the IDA PCAS product (OLP 10) and the PHTRP001 (RP001) processing. The IRAS 60μm flux is 10.576Jy. Δ gives the relative deviation from the model in %.

Det	cwl (μm)	OLP 10	RP001	Model	Δ (RP001)
C1	60.0	7.449	7.643	12.035	-36.49
C1e	60.0	8.866	–	12.035	–

4. CONCLUSIONS

4.1. PHT-S Chopped Spectroscopy

The introduction of the bi-weight mean of the pair-wise difference signals has resulted in smoother spectra giving better agreement with the model stellar spectra, and improving further on the $<$10% absolute accuracy achieved for the IDA products. The reduction of noise due to glitches in the continuum provides more reliable identification of weak PAH features and atomic lines (e.g. NGC1068).

4.2. PHT-C Mini-maps

For mini-maps, the flux densities can now be read directly from the PGAI product header and need not be reconstructed from the raster. A full analysis of many observations, comparing the results with model spectra and IRAS flux densities, has confirmed the OLP V10 calibration accuracies and has led to the following conclusions:

- C100 photometry gives reliable photometry ($<$ 30 %) down to fluxes as low as 50 mJy. However, this may depend on the cirrus confusion level, and hence the absolute surface brightness.
- C200 photometry appears to become unreliable below a flux level of 100 mJy. The absolute level may depend on the actual cirrus confusion noise of the field.
- For extended sources, the point source PSF factors used for flux reconstruction will result in flux densities which are lower than the actual values.

ACKNOWLEDGEMENTS

The UKIDC at RAL is funded by the UK Particle Physics and Astronomy Research Council.

REFERENCES

Ábrahám P. et al., 2002, Proceedings of the Conference "The Calibration Legacy of the ISO Mission", L. Metcalfe et al.(eds), ESA SP-481

Cohen M., 1996, AJ 112, 2274

Hammersley P. L., et al., 1998, A&AS 128, 207

Klaas U., Wilke K., Kiss C., Radovich M. & Richards P., 2000, "Report on the PHT Scientific Validation for OLP Version 9.0", SAI/2000-014/Rp, Version 2.0, p225

Klaas U., & Richards P.J., 2002, Report on the Scientific Validation of PHT OLP version 10.0, version 1.0, 09-April-2002, http://www.iso.vilspa.esa.es/users/expl_lib/PHT_list.html

Klaas U., et al., 2002, this volume

Laureijs R. J., 1999, Point Spread Function Fractions Related to the ISOPHOT C100 and C200 Arrays, IDC PHT Internal Calibration Report

Laureijs R. J., Klaas U., Richards P. J., Schulz B. & Ábrahám P., 2002, ISO Handbook Vol IV: PHT - The Imaging Photo-Polarimeter.

Richards P. J. et al., 2002, Proceedings of the Conference "The Calibration Legacy of the ISO Mission", L.Metcalfe et al.(eds), ESA SP-481

Roche P. F., Aitken D. K., Smith C. H. & Ward M. J., 1991, MNRAS, 248, 606

P32TOOLS: REDUCTION OF ISOPHOT P32 OVERSAMPLED MAPS

Bernhard Schulz[1,2], Nanyao Lu[1], Sibylle B. Peschke[2], Carlos Gabriel[2,3], Iffat Khan[1], and René J. Laureijs[2,4]

[1] IPAC/Caltech, 770 S Wilson Ave, MC 100-22, Pasadena, CA 91125, USA
[2] ISO Data Centre, European Space Agency, Villafranca del Castillo, P.O. Box 50727, 28080 Madrid, Spain
[3] XMM/Newton Science Operations Centre, European Space Agency, Villafranca del Castillo, P.O. Box 50727, 28080 Madrid, Spain
[4] Astrophysics Division, ESA-ESTEC, Postbus 299, NL 2200 AG Noordwijk, The Netherlands

ABSTRACT

During the ISO mission, the ISOPHOT instrument has collected more than 1100 observations in oversampled mapping mode (AOT PHT32) in the wavelength range of 45 to 240 microns. The observations comprise mapping of small and large extended regions, but also faint point sources. PHT32 observations are affected by strong signal transients due to flux changes generated by the relatively fast chopper movement. A program described by Tuffs & Gabriel (2002), was developed to correct for these effects. It was integrated in the ISOPHOT Interactive Analysis (PIA) via a graphical user interface (GUI), so that most aspects of the processing can be addressed in a coherent and user friendly environment. The resulting package "P32Tools" was introduced to the user community at three hands-on workshops on PHT32 processing held in spring 2001. The hands-on experience from these workshops lead to further improvements. Here we present an overview of the functionalities of the final release of this new software.

Key words: ISO – data reduction

1. INTRODUCTION

Most of the P32 data cannot be satisfactorily reduced in a standard fashion because detector transients affect all readouts as a result of the relatively short durations of individual chopper steps. As described by Tuffs & Gabriel (2002), a dedicated algorithm has been developed for correction. The program uses all the readouts to estimate corrected signals by iteratively fitting a detector transient model. The model is fairly complex, involving a dozen tunable parameters per detector pixel. To "hide" much of this complexity from the user, while giving him the necessary control over the data reduction, a graphical user interface has been developed (Lu et al. 2002a). Both parts together form a software package called P32Tools, that is run as ad-don to the PHOT Interactive Analysis (PIA) (Gabriel et al. 1997).

There are 5 main steps to follow in using P32Tools: i) input of an Edited Raw Data (ERD) measurement into the P32Tools data buffer, ii) data structure initialization, iii) working with the **Main P32 Processing** window where maps can be examined and all-pixel transient model fits are initiated, iv) entering the **Inspect Single Pixel** window to examine more closely the time line of an individual detector pixel or fine-tune the transient model, and finally v) output the transient-removed data to PIA or construct a final map and save it to a FITS file. In the following, we highlight some of the most useful features at each of these steps. More information can be found in the on-line `help` facility of the interface and in the proceedings of the "ISOPHOT Workshop on P32 Oversampled Mapping" Feb/Mar 2001, Villafranca, Spain & Pasadena, USA, (ESA SP-482) eds. B. Schulz, N. Lu & S.B. Peschke. The final version 2.0 of P32Tools can be downloaded via the PIA homepage at:
`http://www.iso.vilspa.esa.es/manuals/PHT/pia/-pia.html`,
either separately or packaged together with PIA.

2. DATA INPUT

P32Tools expects the measurement to be already loaded into the ERD buffer of PIA. As a further preparation, the accompanying FCS measurements should already be processed to SCP level according to standard rules before starting the program. Otherwise default responsivities will be used for map making and display (see Gabriel et al. 1997 and Laureijs et al. 2001). P32Tools can be started either by a menu button if you are running PIA V10 or above, or by typing `pia_erd2map` at the IDL prompt within your PIA session. This pops up a **Measurement Selection** dialog.

3. INITIALIZATION

After the file selection, the `Data Initialization Options` window is presented. Along with some information about the measurement, it offers three options that, however, should be left in their default positions, unless for special investigations/debugging. Accepting these selections with the `OK` button starts the initialization of the internal data structures, including construction of natural grids and first-stage deglitching as described by Tuffs & Gabriel (2002).

4. THE MAIN P32 WINDOW

The initialization ends with the appearance of the **Main P32 Processing** window as shown in Fig. 1. Parameters identifying the measurement are displayed at the top. The **SHOW** section below allows to display contour maps of individual detector pixels (`Pixel Map`), the "natural grid" (`Grid`), the contents of FITS-header (`Header`), and compact status file (`Com.`

`Status`), and a map (`Display Map`) according to the options specified in the **Map Display Options** window (Fig. 2). The window is accessed by a button of the same name. The options include if and how flux calibration should be done, if data between satellite slews should be included, which pixels should be combined and whether a flat fielding correction is required [1].

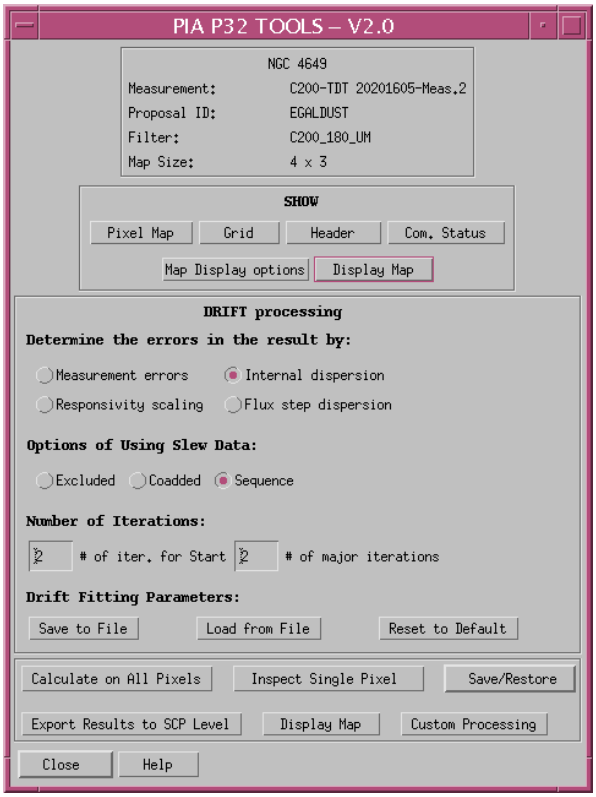

Figure 1. An illustration of the **Main P32 Processing** *window.*

In the following section of the **Main P32 Processing** window, a few basic parameters for the transient modeling algorithm are set. These determine i) how the uncertainties are calculated that are used for the model fit, ii) how and whether the data during slews between raster points are used and iii) the number of iterations allowed for the determination of the start conditions and generally for the model fit. The three buttons at the bottom of this section enable the management of entire sets of model parameters, i.e. to `Save to File`, `Load from File`, or `Reset to Default` the 12 parameters that exist for each detector pixel. Working on the parameters of individual detector pixels requires to enter the **Inspect Single Pixel** dialog (see Sect. 5) via the corresponding button in the section below.

Here a couple of further action buttons are grouped together:

[1] Note that these options affect the display only. The underlying data buffer, which may be exported to PIA, is kept in units of V/s without having the signal linearization correction applied.

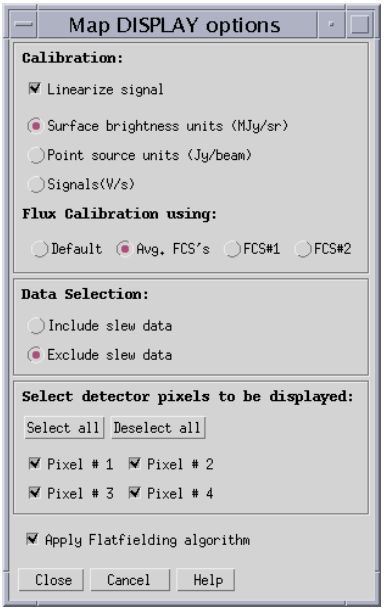

Figure 2. An illustration of the **Map Display Option** *window.*

The button `Calculate on All Pixels` fits the transient model with its current parameter settings to the data of each detector pixel. This procedure is typically one of the first activities after loading the data.

After the measurement has been inspected and has been worked on via the neighboring **Inspect Single Pixel** button, one may want to choose to break the fitting process into certain ranges of data in a preprogrammed way. This is done via the `Custom Processing` dialog and is useful to circumvent a limitation of the model, which results in excessive memory effects after strong changes from high to low flux. This condition typically arises with strong point sources at the centre.

With `Save/Restore` the entire data buffer can be stored on disk or loaded back into memory. This feature is particularly useful for processing data in separate parts, for instance pixel by pixel. Then backup copies of the different reduction stages can be made in case of a software problem along the way. It is also useful for exploring several flavors of processing using a common starting point. It should be noted that for technical reasons, saving data does not save as much time as could be assumed. Once having closed the **Main P32 Processing** window, the original measurement must be loaded and initialized again, before the saved version can be restored.

The `Display Map` button leads to the same map as described in Sect. 4. Instead of deriving the map in this way, the data can be exported back to the SCP buffer of PIA (see Sect. 6), using `Export Results to PIA/SCP`.

5. INSPECT INDIVIDUAL PIXELS

5.1. The Inspect Signals per Pixel

The **Inspect Signals per Pixel** window shown in Fig. 3 provides a facility to visualize the results of a fit more closely,

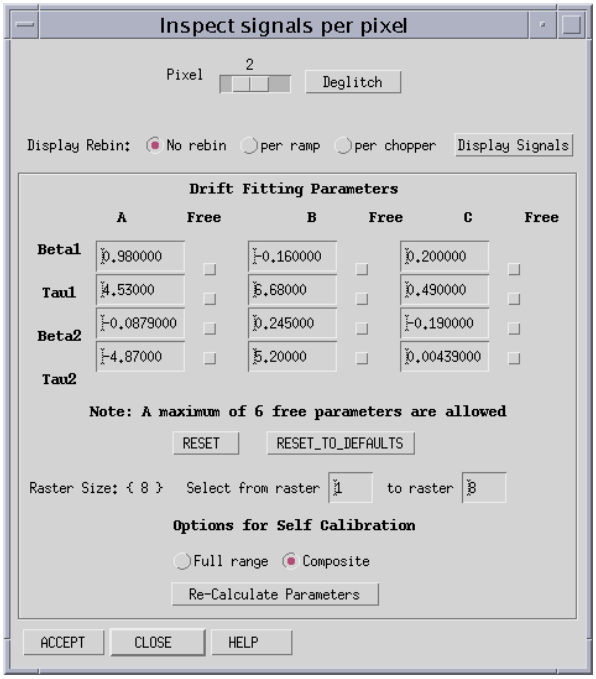

Figure 3. An illustration of the **Inspect Signals per Pixel** *window.*

working on one pixel at a time. It allows for further data cleaning (e.g., deglitching, see Sect. 5.3) and manual or automatic tweaking of detector parameters (see Schulz et al. 2002 for examples on self calibration).

Selection of a pixel is facilitated by a sliding bar near the top of the window. The **Deglitch** button on the right leads to a corresponding dialog, which is covered in Sect. 5.3. This is typically one of the first activities after starting to work on individual pixels.

The data sequence (or time line) of the selected pixel can be displayed by clicking the `Display Signal` button. The data sequence can also be displayed after being rebinned per integration ramp (`per ramp`) or per chopper step (`per chopper`). Some rebinning is useful if the data are noisy or the number of data points slows down the display. Note that rebinning is done using only valid data points.

The transient model parameters for the selected detector pixel are displayed as a matrix of 4 rows by 3 columns. These parameters are defined in Tuffs & Gabriel (2002). Each parameter is associated with a `free` flag. If none is set, the `Recalculate Parameters` button at the bottom of the window just fits the transient model to the detector signal. If at least one free flag is checked, the so-called self calibration mode is entered. Here the selected parameters together with the modeled signal are varied to give the best fit to the detector data. If parameter fitting does not converge, the two buttons below the parameter matrix provide a shortcut to reset the parameters to the values presently in the main P32 window (`Reset`) or to their default values (`Reset to Defaults`). Note that the buttons act only on the detector pixel currently selected.

A working data range is specified by indicating the start and end points within the raster in two fields further down (`Select from raster / to raster`) This range determines which data are displayed or acted upon by the deglitcher and the fitting process.The total number of available raster points is shown on the left between curly brackets.

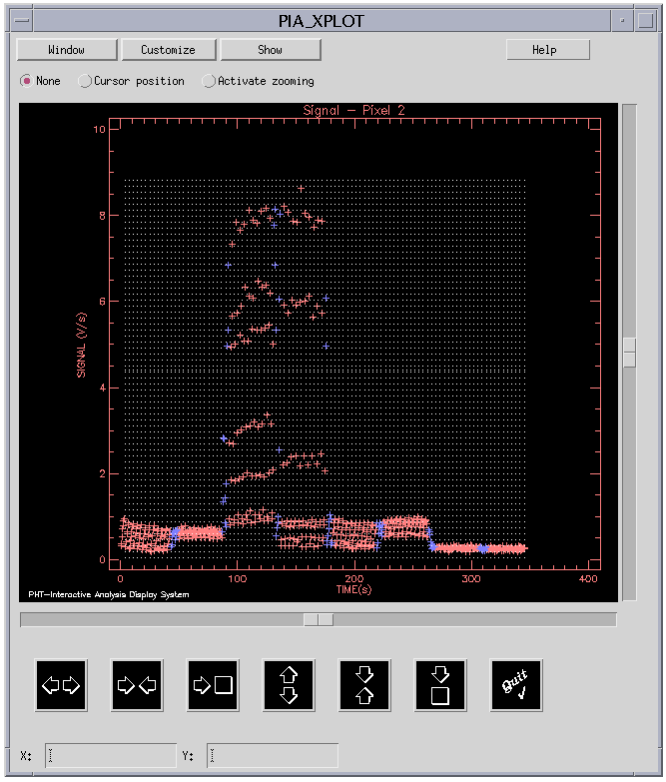

Figure 4. Display of a pixel data sequence with the option of rebinning per chopper step.

A `Full Range` self calibration fits the transient model to all signals in the sequence of raster points. This can be very time consuming. A considerable shortening of processing time is achieved by limiting the data range to one raster point only and averaging all signals measured at the same chopper position. In this mode, the model is fitted to the few remaining data points, which are interpreted as the average reaction of the detector signal to the sequence of fluxes seen during each chopper sweep. This self calibration mode is selected via the `Composite` button. For both options, the `Re-calculate Parameters` button triggers the fitting process.

Finally, the `Accept` button closes the **Inspect Single Pixel** dialog and updates the signal and parameter buffers of the **Main P32 Processing** window. No matter how many pixels have been worked on, upon accepting, the buffers of all pixels are updated. The `Close` button leaves the **Inspect Single Pixel** window without updating the parameters in the **Main P32 Processing** window. However, the dialog can only be closed after turning off any free flags.

5.2. Signal Display

Fig. 4 shows how the display of a single pixel signal appears. Data points taken at a raster position are shown in red and those taken during telescope slews in blue. Without rebinning, any de-selected data points would show as yellow dots. Evenly-spaced dotted vertical lines in the plot mark the beginning of a chopper sweep. For convenience the same display facility is used, as in PIA, allowing to easily zoom for closer inspection (see PIA Users Manual).

5.3. Deglitching

Fig. 5 shows the dialog appearing upon pressing the `Deglitch` button in the **Inspect Single Pixel** window. The appearance is similar to the standard signal display. Valid signals are shown as red squares, while de-selected data show as yellow crosses. Dotted vertical lines indicate the beginning of a chopper sweep and valid slew data points are marked in blue. On the top-right corner of the window are a number of quick navigation and scaling buttons. There are also several display options for the data points. The **Manual Deglitching** buttons allow to de-select and re-select data points using the mouse pointer. This is useful after running the automatic deglitcher described below, to weed out any "stubborn"glitches that were not caught.

The fields along the bottom row of the window contain parameter values for the automatic deglitcher, that are described in detail by Peschke & Tuffs (2002). The `Deglitch` button runs the algorithm, which leads to an update of the display. It is important to note that any further run of the algorithm starts again with the initial dataset that is present when the dialog is started and also discards any manual de-selections. Only leaving the dialog via `EXIT` commits the changes to the main buffer. Leaving via `Quit` discards them.

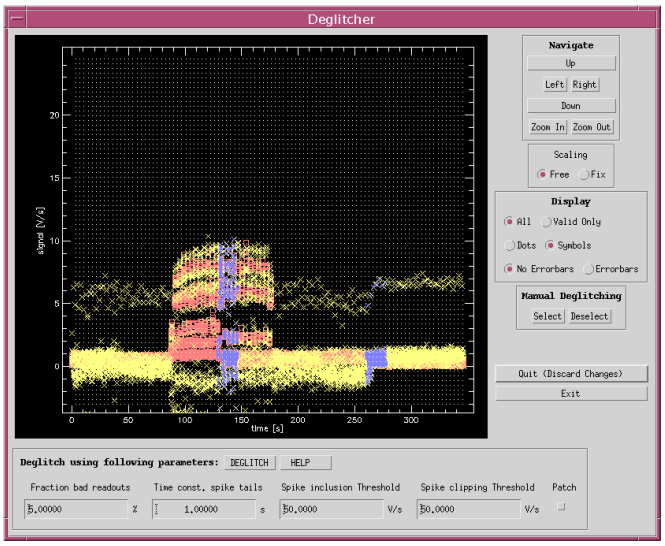

Figure 5. An illustration of the **deglitching window** *where a manual deglitcher and an auto deglitcher are available.*

6. SAVING RESULTS AND DATA OUTPUT

Once a satisfactory model fit has been found for all pixels, a map can be generated directly by P32Tools via the `Display Map` button. The process uses the options set in the **Map Display Options** dialog (see Sect. 4). To make use of the larger number of options to produce maps in PIA and further processing possibilities (e.g. the IMAP tool at SPD level, Lu et al. 2002b), the deglitched and transient-corrected data can be exported to the SCP buffer of PIA using the `Export Results to PIA/SCP` button.

ACKNOWLEDGEMENTS

We are grateful to the P32 workshop participants whose comments have helped us in improving this user interface substantially. This work was supported in part by an ISO grant from the US National Aeronautics and Space Administration, and carried out at the Infrared Processing and Analysis Center, the Jet Propulsion Laboratory of the California Institute of Technology, and the ISO Data Centre of the European Space Agency.

REFERENCES

Gabriel, C., Acosta-Pulido, J., Heinrichsen, I., Morris, H., Tai, W.-M., 1997, in ASP Conf Ser. Vol 125

Laureijs, R.J., Klaas, U., Richards, P.J., Schulz, B., Ábrahám, P., 2001, ISO Handbook, Volume V: PHT–The Imaging Photo-Polarimeter, Version 1.2

Lu N., Khan I., Schulz B., Peschke S.B., Laureijs, R.J., Gabriel C., 2002a, ESA SP-482

Lu N., Hur M., & Li J., 2002b, ESA SP-482

Peschke S., Schulz, B., 2002, ESA SP-482

Peschke S., & Tuffs R. J., 2002, ESA SP-482

Schulz B., Tuffs, R.J., Laureijs, R.J., Gabriel, C., Khan, I., 2002, ESA SP-482

Tuffs R. J. & Gabriel, C., 2002, ESA SP-482

PHOTOMETRIC MAPPING WITH ISOPHOT USING THE "P32" ASTRONOMICAL OBSERVATION TEMPLATE

Richard J. Tuffs[1] **and Carlos Gabriel**[2]

[1] Astrophysics Division, Max-Planck-Institut für Kernphysik, Saupfercheckweg 1, 69117 Heidelberg, Germany.
Richard.Tuffs@mpi-hd.mpg.de
[2] XMM-Newton Science Operations Centre, European Space Agency, Villafranca del Castillo, P.O. Box 50727, 28080 Madrid, Spain

ABSTRACT

The "P32" Astronomical Observation Template (AOT) provided a means to map large areas of sky (up to 45×45 arcmin) in the FIR at high redundancy and with sampling close to the Nyquist limit using the ISOPHOT C100 (3×3) and C200 (2×2) detector arrays on board ISO. However, the transient response behaviour of the Ga:Ge detectors, if uncorrected, can lead to severe systematic photometric errors and distortions of source morphology on maps. Here we demonstrate the photometric and imaging performance of an algorithm which can successfully correct for transient response artifacts in P32 observations.

Key words: ISO

1. INTRODUCTION

From the point of view of signal processing and photometry diffraction-limited mapping in the FIR with cryogenic space observatories equipped with photoconductor detectors poses a particular challenge. In this wavelength regime the number of pixels in detector arrays is limited in comparison with that in mid- and near-IR detectors. This means that more repointings are needed to map structures spanning a given number of resolution elements. Due to the logistical constraints imposed by the limited operational lifetime of a cryogenic mission, this inevitably leads to the problem that the time scale for modulation of illumination on the detector pixels becomes smaller than the characteristic transient response timescale of the detectors to steps in illumination. The latter timescale can reach minutes.

Unless corrected for, the transient response behaviour of the detectors will lead to distortions in images, as well as to systematic errors in the photometry of discrete sources appearing on the maps. In general, these artifacts become more severe and more difficult to correct for at fainter levels of illumination, since the transient response timescales increase with decreasing illumination. Compared to the IRAS detectors, the ISOPHOT-C detectors (Lemke et al. 1996) on board the Infrared Space Observatory (ISO; Kessler et al. 1996) had relatively small pixels designed to provide near diffraction limiting imaging. ISOPHOT thus generally encountered larger contrasts in illumination between source and background than IRAS did, making the artifacts from the transient response more prominent, particularly for fields with faint backgrounds.

A further difficulty specific to mapping in the FIR with ISO was that, unlike IRAS, the satellite had no possibility to cover a target field in a controlled raster slew mode. This limited the field size that could be mapped using the spacecraft raster pointing mode alone, since the minimum time interval between the satellite fine pointings used in this mode was around 8 s. This often greatly exceeded the nominal exposure time needed to reach a required level of sensitivity (or even for many fields the confusion limit). Furthermore, the angular sampling and redundancy achievable using the fine pointing mode in the available time was often quite limited, so that compromises sometimes had to be made to adequately extend the map onto the background.

A specific operational mode for ISO - the "P32" Astronomical Observation Template (AOT) - was developed for the ISOPHOT instrument to alleviate these effects (Heinrichsen et al. 1997). This mode employed a combination of standard spacecraft repointings and rapid oversampled scans using the focal plane chopper. The technique could achieve a Nyquist sampling on map areas of sky ranging up to 45×45 arcmin in extent (ca. 70×70 FWHM resolution elements) on timescales of no more than a few hours. In addition to mapping large sources, the P32 AOT was extensively used to observe very faint compact sources where the improved sky sampling and redundancy alleviated the effects of confusion and glitching.

In all, over 6% of the observing time of ISO was devoted to P32 observations during the 1995-1998 mission, but the mode could not until now be fully exploited scientifically due to the lack of a means of correcting for the complex non-linear response behaviour of the Ge:Ga detectors. Here we describe the photometric performance of a new algorithm which can successfully correct for the transient response artifacts in P32 observations. This algorithm forms the kernel of the "P32TOOLS" package, which is now publically available as part of the ISOPHOT Interactive Analysis package PIA (Gabriel et. al 1997; Gabriel & Acosta-Pulido 1999). The user interface of P32TOOLS and its integration into PIA is described by Lu et al. (2002) and by Schulz et al. (2002a, 2002b). Information on the algorithm itself, as well as the first scientific applications, can be found in Tuffs et al. (2002) and Tuffs & Gabriel (2002).

2. PHOTOMETRIC PERFORMANCE

In general the corrections in integrated flux densities made by the algorithm depend on the source brightness, structure, the source/background ratio, and the dwell time on each chopper

Proceedings of the Symposium *"Exploiting the ISO Data Archive - Infrared Astronomy in the Internet Age"*,
24–27 June 2002, Sigüenza, Spain (C. Gry, S. B. Peschke, J. Matagne et al. eds., ESA SP-511)

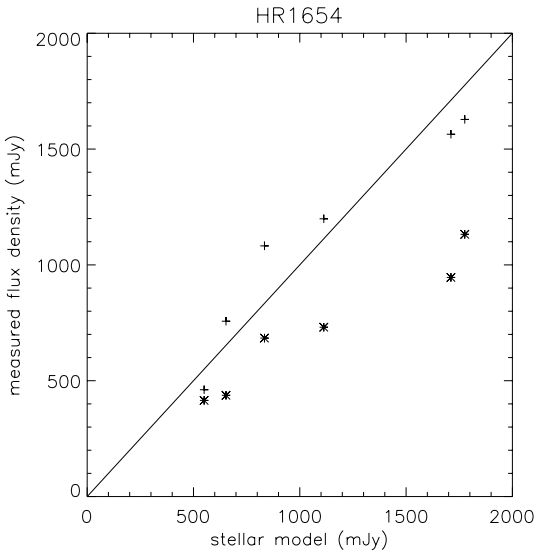

Figure 1. The measured integrated flux densities of the faint standard star HR 1654 plotted against the predicted flux densities from a stellar model. The observations were done in various filters using the C100 detector. The photometry derived with and without processing with P32TOOLS is shown with stars and crosses, respectively.

plateau. The largest corrections are for bright point sources on faint backgrounds.

Here we give as an example results achieved for the faint standard star HR 1654. This source was not used in the determination of the detector model parameters, so it constitutes a test of the photometric performance of ISOPHOT in its P32 observing mode. The derived integrated flux densities, with and without correction for the transient response behaviour of the C100 detector, were compared in Fig. 1 with predicted flux densities from a stellar model. The corrected photometry is in reasonable agreement with the theoretical predictions. As expected, there is a trend for observations with larger detector illuminations to have larger corrections in integrated photometry.

A good linear correlation is also seen between integrated flux densities of Virgo cluster galaxies (Tuffs et al. 2002), derived from P32 ISOPHOT observations processed using the P32TOOLS algorithm, and flux densities from the IRAS survey (Fig. 2). The interpretation of these measurements constitutes the first science application (Popescu et al. 2002) of P32TOOLS algorithm. The ISOPHOT observations of Virgo cluster galaxies were furthermore used to derive the ratios of fluxes measured by ISO to those measured by IRAS. The ISO/-IRAS ratios were found to be 0.95 and 0.82 at 60 and 100 μm, respectively, after scaling the ISOPHOT measurements onto the COBE-DIRBE flux scale (Tuffs et al. 2002).

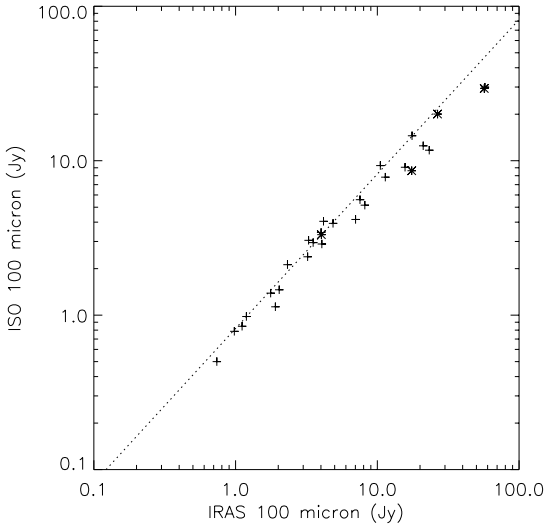

Figure 2. Integrated and colour-corrected flux densities of Virgo cluster galaxies measured in the ISO C100 filter versus the corresponding flux densities measured by IRAS in its 100 μm band (taken from Fig. 7 of Tuffs et al. 2002). The dotted line represents the relation ISO/IRAS=0.82.

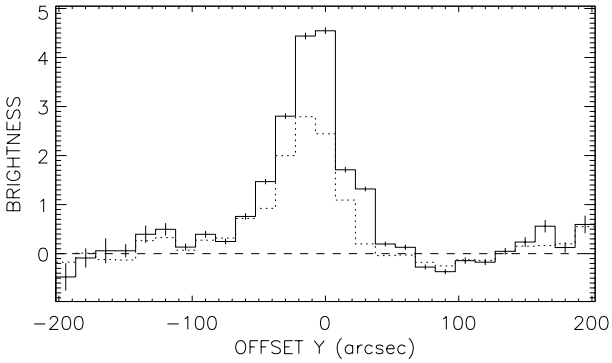

Figure 3. Brightness profiles along the Y spacecraft direction through the standard star HR 1654 at 100 μm. The solid line represents the brightness profile obtained after processing with P32TOOLS, while the dotted line shows the profile derived from identically processed data, but without correction for the transient response of the detector.

Fig. 3 shows an example of a brightness profile through HR 1654 at 100 μm, for data processed with and without the responsivity correction. Some 95% of the flux density has been recovered by P32TOOLS. Without the correction, some 30% of the integrated emission is missing and the signal only reaches 50% of the peak illumination. The local minimum near 60 arcsec in the Y offset is a typical hook response artifact, where the algorithm has overshot the true solution. This happens for rapid chopper sweeps passing through the beam kernel. This is a fundamental limitation of the detector model, which, as described in Sect. 3.1, does not correctly reproduce the hook response on timescales of up to a few seconds. This problem is particularly apparent for downwards illumination steps. The only effective antidote is to mask the solution immediately following a transition through a bright source peak. Another effect of the inability to model the hook response is that the beam profile becomes somewhat distorted.

This also has the consequence, that for observations of bright sources, the measured FWHM can become narrower than for the true point spread function, as predicted from the telescope

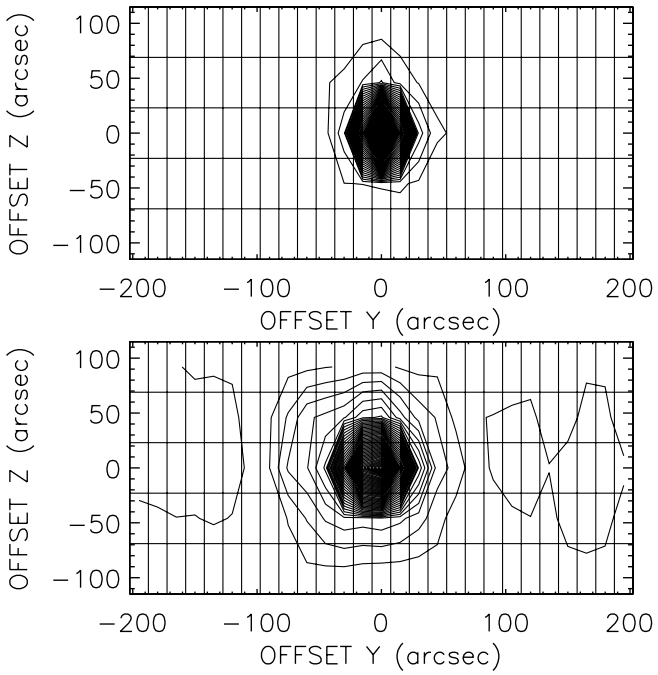

Figure 4. Top: Contour map of Ceres in the C105 filter after responsivity drift correction. 50 linear contours have been plotted between 33 and 2519 MJy/sr. Measured integrated flux density after background subtraction is $98.4\,Jy \pm 0.2\,Jy$ *(random)* $\pm 6\%$ *(systematic). The actual flux density of this standard calibrator (from a stellar model) is 109 Jy. Bottom: Contour map of Ceres in the C105 filter without correction for the transient response behaviour of the detector. 50 linear contours have been plotted between 11.5 and 334 MJy/sr. Measured integrated flux density after background subtraction is* $28.0\,Jy \pm 0.07\,Jy$ *(random)* $\pm 4\%$ *(systematic)*

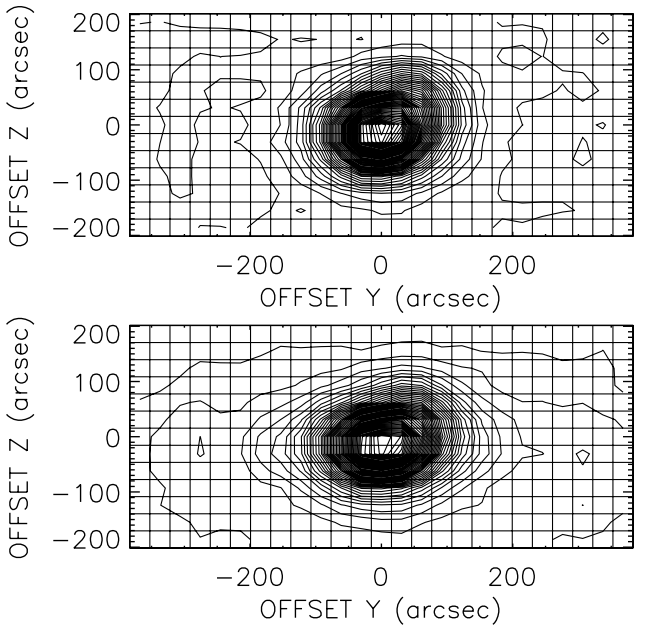

Figure 5. The interacting galaxy pair kpg 347 observed in the C200 filter. Top: after processing with P32TOOLS, Bottom: with identical processing, except that the correction for the transient response behaviour of the detector has been omitted.

optics and pixel footprint. An example of an extremely bright point source showing this effect is given in Fig. 4, depicting maps of Ceres in the C105 filter, respectively made without and with the correction for the transient response of the C100 detector.

Despite the limitations due to the lack of a proper modelling of the hook response, the algorithm can effectively correct for artifacts associated with the transient response on timescales from a few seconds to a few minutes. This is illustrated in Fig. 5 by the maps of the interacting galaxy pair KPG 347 in the C200 filter (again, after and before correction for the transient response of the detector, respectively). The uncorrected map shows a spurious elongation in the direction of the spacecraft Y coordinate, which is almost completely absent in the corrected map. If uncorrected, such artifacts could lead to false conclusions about the brightness of FIR emission in the outer regions of resolved sources. Also visible in the corrected map is a trace of a beam sidelobe.

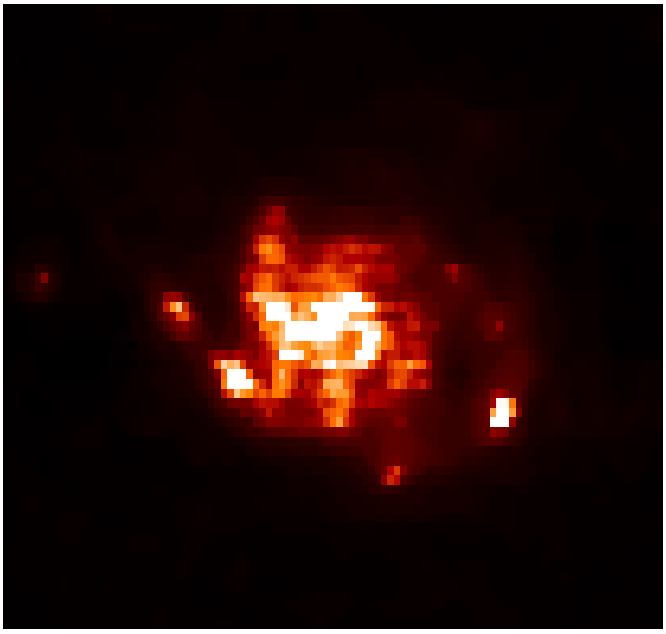

Figure 6. A 27×27 *arcmin field containing the galaxy M101, as mapped in the C100 filter, after processing with P32TOOLS. The map sampling is* 15×23 *arcsec.*

The image of M 101 in Fig. 6, made using the C100 detector with the C100 filter, is given as a state of the art example of what can be achieved with a careful interactive processing of P32 data using P32TOOLS. In addition to the transient response corrections and a masking of residual hook response artifacts, a time dependent flat field has been applied. The spiral structure of the galaxy, with embedded HII region complexes and a component of diffuse interarm emission can clearly be seen.

ACKNOWLEDGEMENTS

This work was supported by grant 50-QI-9201 of the Deutsches Zentrum für Luft- und Raumfahrt. I would like to thank all those who

have helped me in many ways in the development of the algorithm described here. Richard Tuffs would like to thank his colleagues at the Max-Planck-Institut für Kernphysik, in particular Prof. Heinrich Völk, for their support and encouragement. We have also benefited from many useful discussions with Drs. R. Laureijs, S. Peschke and B. Schulz and the team in the ISO data centre at Villafranca, with Prof. D. Lemke and Dr. U. Klaas at the ISOPHOT data centre at the Max-Planck-Institut für Astronomie, and with Drs. N. Lu and I. Khan at the Infrared Processing and Analysis Center.

REFERENCES

Gabriel, C., Acosta-Pulido, J., Heinrichsen, I., Morris, H., & Tai, W-M., in: Astronomical Data Analysis Software and Systems VI, A.S.P. Conference Series, Vol. 125, 1997, Gareth Hunt & H.E. Payne, eds., p. 108.

Gabriel, C., & Acosta-Pulido, J.A., 1999, ESA SP-427, p73.

Heinrichsen, I.H., Gabriel, C., Richards, P., & Klaas, U., 1997, ESA SP-401, p273.

Kessler, M.F., Steinz, J.A., Anderegg, M.E. et al. 1996, A&A 315, L27.

Lemke, D., Klaas, U., Abolins, J., et al. 1996, A&A 315, L64.

Lu, N., Khan, I., Schulz, B., et al. 2002, ESA SP-482, in press

Popescu, C.C., Tuffs, R.J., Völk, H.J., Pierini, D. & Madore, B.F., 2002, ApJ 567, 221.

Schulz, B., Tuffs, R.J., Laureijs, R.J. et al. 2002a, ESA SP-482, in press

Schulz, B., Lu, N., Peschke, S.B. et al. 2002b, this volume

Tuffs, R.J. & Gabriel, C. 2002, ESA SP-482, in press

Tuffs, R.J., Popescu, C.C., Pierini, D., Völk, H.J., Hippelein, H., Heinrichsen, I. & Xu, C., 2002, ApJS 139, 37